

Increased drug permeability of a stiffened mycobacterial outer membrane in cells lacking MFS transporter Rv1410 and lipoprotein LprG

Michael Hohl,¹ ^{1,t,✉} Sille Remm,¹ ^{1#}
 Haig A. Eskandarian,² ² Michael Dal Molin,¹
 Fabian M. Arnold,¹ Lea M. Hürlmann,¹ Andri Krügel,¹
 Georg E. Fantner,³ ³ Peter Sander^{1,4} and
 Markus A. Seeger ^{1*}

¹ Institute of Medical Microbiology, University of Zurich, Zürich, Switzerland.

² Global Health Institute, École polytechnique fédérale de Lausanne, EPFL, Lausanne, Switzerland.

³ Interfaculty Institute for Bioengineering, École polytechnique fédérale de Lausanne, EPFL, Lausanne, Switzerland.

⁴ National Center for Mycobacteria, Zurich, Switzerland.

Summary

The major facilitator superfamily transporter Rv1410 and the lipoprotein LprG (Rv1411) are encoded by a conserved two-gene operon and contribute to virulence in *Mycobacterium tuberculosis*. Rv1410 was originally postulated to function as a drug efflux pump, but recent studies suggested that Rv1410 and LprG work in concert to insert triacylglycerides and lipoarabinomannans into the outer membrane. Here, we conducted microscopic analyses of *Mycobacterium smegmatis* lacking the operon and observed a cell separation defect, while surface rigidity measured by atomic force microscopy was found to be increased. Whereas Rv1410 expressed in *Lactococcus lactis* did not confer drug resistance, deletion of the operon in *Mycobacterium abscessus* and *M. smegmatis* resulted in increased susceptibility toward vancomycin, novobiocin and rifampicin. A homology model of Rv1410 revealed a periplasmic loop as well as a highly conserved aspartate, which were found to be essential for the operon's function.

Accepted 6 February, 2019. *For correspondence. E-mail m.seeger@imm.uzh.ch; Tel. +41 44 634 53 96; Fax +41 44 634 49 06. ^tPresent address: Department of Life Sciences, Imperial College London, London, UK. [#]These authors contributed equally to this work.

Interestingly, influx of the fluorescent dyes BCECF-AM and calcein-AM in de-energized *M. smegmatis* cells was faster in the deletion mutant. Our results unambiguously show that elevated drug susceptibility in the deletion mutant is caused by increased drug influx through a defective mycobacterial cell envelope and not by drug efflux mediated by Rv1410.

Introduction

The pathogenic bacterium *Mycobacterium tuberculosis* is responsible for approximately 1.7 million cases of death every year. In particular, the emergence of multi-drug (MDR) and extensively drug-resistant strains are a global health threat. Mycobacteria are intrinsically resistant against many antibiotics due to their thick and complex outer membrane (Hoffmann *et al.*, 2008). The main constituents of the mycobacterial cell wall are mycolic acids covalently connected to the arabinogalactan layer, and a plethora of glycolipids such as trehalose dimycolates (TDMs) and lipoarabinomannans (LAMs) that interact non-covalently with the mycolic acids (Dhiman *et al.*, 2011). Due to its biological uniqueness, many TB-specific drugs are targeting the assembly of this cell envelope and the biosynthesis of its lipids. The composition and biosynthesis of this formidable cell barrier are well established. In contrast, much less is known about how these lipids are integrated into the cell wall or how the precursors are transported across the cytoplasmic membrane.

The major facilitator superfamily (MFS) transporter Rv1410 (also called P55) is located in the cytoplasmic membrane. Initial studies in *Mycobacterium bovis* have established that Rv1410 shares homology to multidrug efflux proteins and is encoded in a highly conserved two-gene operon together with the lipoprotein LprG (also named Rv1411 or P27) (Bigi *et al.*, 2000). Overexpression of *rv1410* in *Mycobacterium smegmatis* conferred aminoglycoside and tetracycline resistance, which could be reversed in the presence of the protonophore carbonyl cyanide m-chlorophenylhydrazone (CCCP), as well as

the efflux pump inhibitors verapamil and reserpine, suggesting that it functions as a proton-driven drug efflux pump (Silva *et al.*, 2001). *M. bovis* Δ *rv1410* exhibited higher susceptibility toward a number of drugs including rifampicin and clofazimine (Ramon-Garcia *et al.*, 2009), and deletion of the homologous operon in *M. smegmatis* resulted in increased susceptibility toward ethidium (Farrow and Rubin, 2008). Interestingly, the authors of these studies noted altered colony morphology, growth attenuation, cell clumping and hampered sliding motility, suggesting that lack of this operon leads to altered cell surface properties. Furthermore, it was found that LprG is needed for the normal functioning of Rv1410, suggesting that they operate in concert (Farrow and Rubin, 2008). Structural and functional analyses of the lipoprotein LprG permitted insights from a completely different angle. LprG was found to associate with the triacylated Toll-like receptor 2 (TLR2) agonists LAM, lipomannan and phosphatidylinositol mannoside (PIM). This notion was corroborated by a structure of LprG co-crystallized in complex with the LAM precursor Ac₁PIM₂, revealing a hydrophobic pocket accommodating the three alkyl chains of the lipid (Drage *et al.*, 2010). Surface plasmon resonance (SPR) studies using purified LprG and triacylated lipids including LAM further confirmed this molecular interaction and revealed a secondary sugar-binding site outside of the hydrophobic pocket, resulting in a particularly high affinity of LprG for LAMs (Shukla *et al.*, 2014). Very recent studies in addition revealed molecular interactions of purified LprG with TLR2 (Shukla *et al.*, 2018). Virulence of *M. tuberculosis* Δ *lprG* in BALB/c mice was clearly attenuated and the mutant exhibits impaired macrophage entry and fails to inhibit phagosome–lysosome fusion (Bigi *et al.*, 2004). Attenuated virulence was initially proposed to be caused by decreased surface localization of LAMs, implying that LprG transports LAMs from the plasma membrane into the cell envelope (Gaur *et al.*, 2014; Shukla *et al.*, 2014). However, a recent study refuted this hypothesis by showing that the deletion mutant also multiplies slower in mice lacking key elements of either the innate or adaptive immune system, which are thought to be triggered by LAMs (Martinot *et al.*, 2016). Lipidome analyses revealed that deletion of the *lprG-rv1410* operon leads to intracellular accumulation of triacylglycerides (TAGs) and that overexpression of the locus in turn increases the levels of TAGs in the culture medium (Martinot *et al.*, 2016). This pointed at a metabolic defect in the deletion mutant being responsible for decreased virulence in mice and further lent support to the operon's role in the transport of triacylated lipids. In a very recent study, LprG was found to interact with various periplasmic proteins, including mycolyltransferase Ag85A, which catalyzes the formation of TDM in the cell wall (Touchette *et al.*, 2017).

The available data about the *lprG-rv1410* operon of *M. tuberculosis* and the homologous operons of other mycobacterial species (henceforth called collectively *lprG-mfs* operons) so far mainly addressed the function of the lipoprotein LprG, namely its possible role in the transport of LAMs and TAGs from the plasma membrane into the outer membrane and the immunological consequences of a reduced LAM exposure at the surface of the mycobacterial cell. By contrast, comparatively little is known about the function of the proton-driven transporter Rv1410, in particular with regard to its suggested dual role of being a drug efflux pump as well as a lipid transporter. To shed light on the function of Rv1410, we cloned, expressed and purified Rv1410 and studied its interaction with the lipoprotein LprG *in vitro*. Deletion mutants of the *lprG-mfs* operon were constructed in *M. smegmatis* and in *Mycobacterium abscessus* and evaluated for drug susceptibility and transport of fluorescent dyes to resolve Rv1410's role as drug efflux pump. A homology model of Rv1410 was generated, which formed the basis to functionally characterize a conserved aspartate and a periplasmic loop. Finally, cell surface properties and morphology of the *M. smegmatis* deletion mutant were studied using AFM and microscopy techniques offering insight into the biophysical role of the Rv1410 operon.

Results

Homology model of Rv1410

According to the transporter classification database (<http://www.tcdb.org>), Rv1410 belongs to the MFS subclass drug:H⁺ antiporter-2 (DHA2), which mainly consists of drug efflux pumps. DHA2 members all feature 14 transmembrane helices (TMs), namely two bundles of six TMs, which are common to all MFS transporters, and an additional helix pair placed between these bundles (6+2+6 TMs) (Reddy *et al.*, 2012). Other well characterized DHA2 family members are the drug efflux pumps LfrA from *M. smegmatis* (Sander *et al.*, 2000) and QacA from *Staphylococcus aureus* (Paulsen *et al.*, 1996a). Currently, there is no structure available for a DHA2 transporter. The closest structural homologue of Rv1410 is PepT_{S02} of *Shewanella oneidensis* (sequence identity of 14.2% and coverage of 0.844 according to the SwissModel server), an MFS transporter belonging to the subfamily of proton-dependent oligopeptide transporters, which share the 6+2+6 helical arrangement with Rv1410 (Guettou *et al.*, 2013; Newstead, 2015). Therefore, a homology model was generated based on the coordinates of PepT_{S02} (PDB ID: 4LEP) using the SwissModel server (Biasini *et al.*, 2014) (Fig. 1A). The model contains the classical fold common to all MFS transporters comprising TM1–12 and

the two additional helices (called HA and HB) connecting the two lobes of the transporter, whose functional role is currently unclear (Newstead, 2015). Interestingly, Rv1410 contains a periplasmic loop consisting of 34 amino acids placed between TM11 and TM12 (Fig. 1A), which is not present in any of the known MFS structures and whose function is unknown.

A sequence alignment involving Rv1410, the *L. lactis* drug efflux pump LmrP and the *Escherichia coli* drug efflux pump MdfA – both belonging to the DHA1 family of

MFS transporters containing 12 TMs – along with PepT_{S_O2} and LfrA revealed a highly conserved aspartate (D70 in Rv1410) (Fig. 1B). This aspartate is part of the conserved motif A (consensus sequence GrLaDrGGrRRV) located at the cytoplasmic loop between TM2 and TM3 in all MFS transporters (Fig. 1A) (Paulsen *et al.*, 1996b). Mutation of this aspartate into cysteine in LmrP or alanine in MdfA, respectively, was shown to completely abrogate drug efflux in these transporters (Mazurkiewicz *et al.*, 2004; Sigal *et al.*, 2006). A double electron–electron resonance

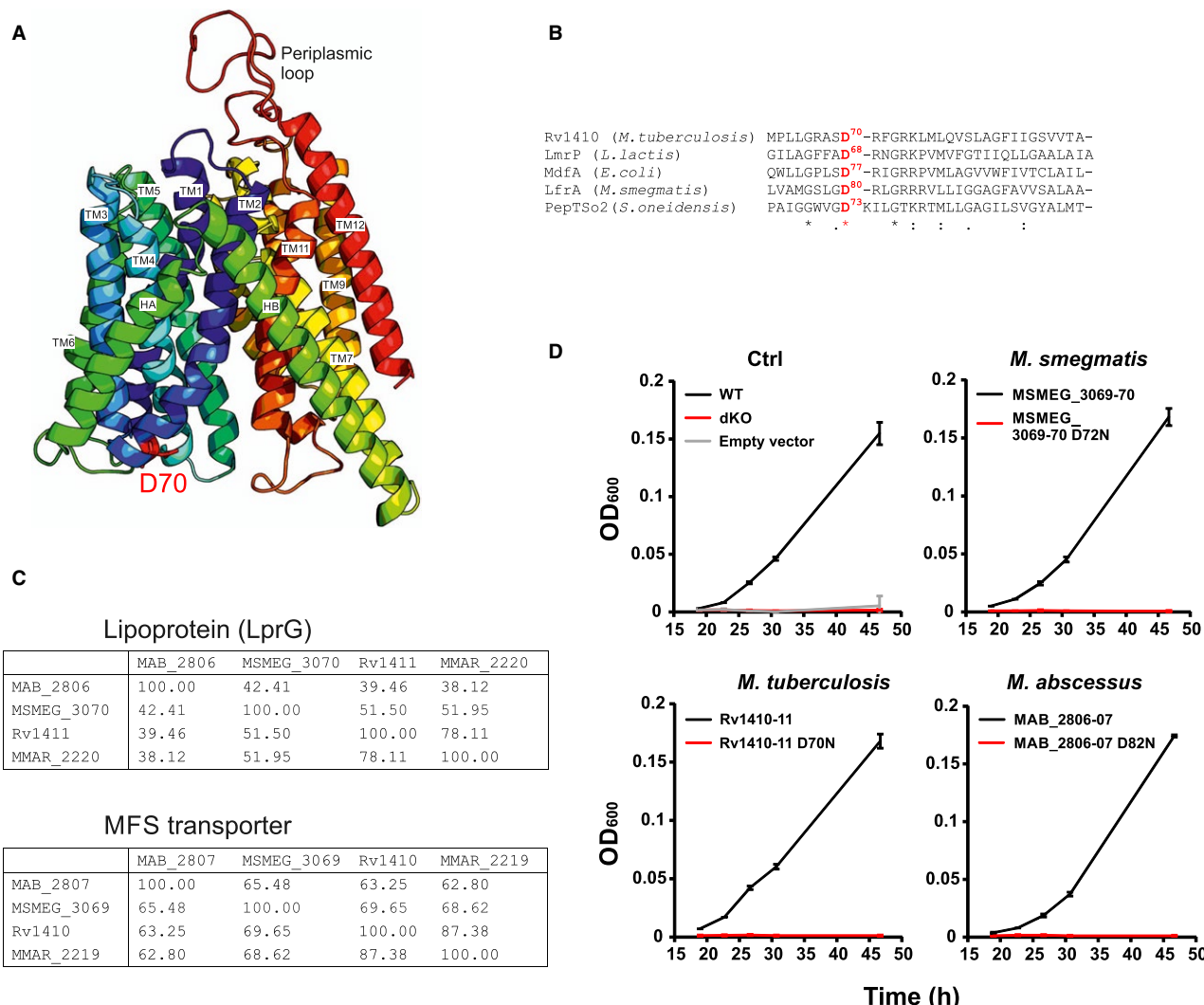


Fig. 1. Homology model of Rv1410 and conservation of the *lprG-mfs* operon.

A. Homology model of Rv1410 based on the coordinates of PepT_{S_O2} (PDB ID: 4LEP). A highly conserved aspartate (D70) and a unique periplasmic loop between TM11 and TM12 are labeled.

B. Sequence alignment of MFS transporters showing the conserved motif A between TM2 and TM3. An aspartate residue (highlighted in red) is strictly conserved, and was mutated to asparagine to inactivate the transporters (DtoN mutation).

C. Conservation of LprG and the MFS transporter among different mycobacterial species. MAB, *M. abscessus*; MSMEG, *M. smegmatis*; Rv, *M. tuberculosis*; MMAR, *M. marinum*. The numbers correspond to amino acid sequence identities.

D. *M. smegmatis* dKO was complemented with *lprG-mfs* operons from *M. smegmatis* (MSMEG_3069-70), *M. tuberculosis* (rv1410-11) or *M. abscessus* (MAB_2806-07) and grown in liquid media containing vancomycin. Complementation with operons carrying the inactivating DtoN mutations in the respective MFS transporters was performed as well. As a control (Ctrl), wild-type cells (WT), *M. smegmatis* dKO alone (dKO) or complemented with an empty vector were analyzed. [Colour figure can be viewed at wileyonlinelibrary.com]

(DEER) study of LmrP revealed that this aspartate plays a key role in coupling substrate transport to the influx of protons (Masureel *et al.*, 2014). We therefore mutated this conserved aspartate into asparagine (henceforth called DtoN mutation), to obtain an inactive Rv1410 variant that is uncoupled from the proton gradient.

*Deletion of the lprG-mfs operon in *M. abscessus* and *M. smegmatis* increases drug susceptibility*

Mycobacterium abscessus is a major cause of infections in cystic fibrosis patients and is notoriously difficult to treat because of its intrinsic resistance toward many antibiotics including first-line TB drugs (Brown-Elliott *et al.*, 2012; Mougari *et al.*, 2016; Rominski *et al.*, 2017; Luthra *et al.*, 2018). Genetic deletion of the *lprG-mfs* operon (Δ MAB_2806-07, henceforth called dKO) resulted in a pronounced increase of antibiotic susceptibilities toward six antibiotics, including tetracycline, rifabutin and vancomycin (Table 1). Complementation studies of the deletion mutant were carried out using the integrative vector pFLAG (Arnold *et al.*, 2018), harboring the coding sequences of LprG (MAB_2806), the MFS transporter (MAB_2807) or the entire operon under the control of a constitutively active promoter. Complementation with the entire operon fully rescued the dKO mutant. In contrast, MICs were identical to the vector control if the complementation vector carried LprG alone or the operon with the MFS transporter carrying the D82N mutation respectively. Interestingly, complementation with the MFS transporter alone almost completely reversed drug susceptibility.

The *lprG-mfs* operon was also deleted in *M. smegmatis* (Δ MSMEG_3069-70, henceforth called dKO), as described previously (Farrow and Rubin, 2008), and the resulting mutant was found to exhibit increased susceptibility toward vancomycin, rifabutin and novobiocin (Table 2). Complementation with the MSMEG_3069-70 operon fully reversed drug susceptibility to wild-type level, whereas the D72N mutation introduced in the MFS transporter fully abrogated its function. Complementation with the MFS transporter MSMEG_3069 partially reversed drug susceptibility, but complementation with *lprG* (MSMEG_3070) did not.

In summary, lack of the *lprG-mfs* operon strongly increases intrinsic drug susceptibility in *M. abscessus* and to a lesser degree in *M. smegmatis*. In both operons, the MFS transporters play a dominant role, because their expression partially reversed drug susceptibility.

The lprG-mfs operon is highly conserved in mycobacteria

High degrees of amino acid identities ranging between 38–78% for LprG and 63–87% for the MFS transporter

among different mycobacterial species suggest a conserved function of the operon (Fig. 1C). In agreement with this notion, complementation with the wild-type operons from either *M. smegmatis*, *M. tuberculosis* or *M. abscessus* fully rescued the growth defect of *M. smegmatis* dKO in the presence of vancomycin, rifampicin or novobiocin (Figs 1D and S1). The mutations D70N (*M. tuberculosis*), D72N (*M. smegmatis*) and D82N (*M. abscessus*) in Rv1410 and its homologues fully inactivated the transporters and thus the operon. Based on these observations, we decided to study the function of *M. tuberculosis* Rv1410 and LprG in *M. smegmatis* dKO in greater detail.

Periplasmic loop truncations strongly affect function of Rv1410

The homology model of Rv1410 predicts a periplasmic loop (34 amino acids) between transmembrane helices 11 and 12, which is not present in published MFS transporter structures. To assess its functional role, we generated truncation mutants lacking 10, 18, or 26 amino acids of the loop respectively (Fig. 2A). The *M. smegmatis* dKO strain was complemented with the operon containing wild-type LprG and Rv1410 harboring different loop truncations, and was subjected to antibiotic susceptibility testing. Short and medium loop mutants of Rv1410 were as inactive as the deleterious D70N mutant (Fig. 2D–F). In contrast, the Rv1410 mutant containing the longest loop (i.e. the shortest deletion) was partially active. Its residual activity is similar to the one of LprG containing the previously described V91W mutation (Drage *et al.*, 2010) (Fig. 2D–F). Western blot analysis revealed that the expression of the loop truncation mutants and wild-type Rv1410 were equally strong in *M. smegmatis* (Fig. 2C). Size exclusion chromatography analysis of purified mutant proteins suggested that these mutations did not alter the folding behavior of Rv1410 because the mutant proteins' peaks coincided with the peak of wild-type Rv1410 on SEC (Fig. 2B, Rv1410 purification is explained in more detail in the subsequent section). Together, these results support the hypothesis that the periplasmic loop is involved in transport processes mediated by Rv1410 and LprG.

Purified Rv1410 and LprG do not interact

We hypothesized that the periplasmic loop of Rv1410 may physically interact with LprG, which is known to be attached to the outer leaflet of the cytoplasmic membrane via its lipid anchor. To study a potential interaction at the biochemical level, we individually expressed and purified Rv1410 and LprG. Rv1410 was overexpressed in *E. coli* with a His-tagged GFP fused to its C-terminus.

Table 1. MIC determination of *M. abscessus* dKO (*ΔMAB_2806-07*).

Strain	Antibiotic	Tetracycline	Vancomycin	Rifabutin	Clofazimine	Novobiocin	Ofloxacin
WT	Median	>128	>128	8	0.25	64	64
	Range	(128 to >128)	(>128)	(4–8)	(0.25–0.5)	(32–64)	(32–64)
dKO	Median	16	16	1	0.06	1	4
	Range	(8–16)	(8–16)	(1)	(0.06–0.125)	(1–2)	(4)
EV	Median	16	16	0.5	0.125	0.5	4
	Range	(8–32)	(16–32)	(0.25–0.5)	(0.06–0.125)	(≤0.25–2)	(4–8)
c. <i>mfs</i>	Median	128	>128	4	0.25	32	32
	Range	(128 to >128)	(128 to >128)	(4–8)	(0.25–0.5)	(32–64)	(16–32)
c. <i>lprG</i>	Median	16	16	0.5	0.06	1	4
	Range	(8–16)	(8–32)	(0.5–2)	(0.06–0.125)	(≤0.25–2)	(4–8)
c. <i>lprG-mfs</i>	Median	>128	>128	8	0.5	64	32
	Range	(128 to >128)	(128 to >128)	(4–8)	(0.25–0.5)	(32–64)	(16–64)
c. <i>lprG-mfs</i>	Median	16	32	0.5	0.06	0.5	4
	Range	(16–64)	(8–32)	(0.5–1)	(0.06–0.25)	(≤0.25–1)	(4–8)
DtN	Range						

Complementation (c.) was carried out with the genes of the *lprG-mfs* operon from *M. abscessus*. EV, empty vector control. DtN, MAB2807 D82N. MIC values correspond to µg ml⁻¹ of the respective antibiotics used. Shown are the median and range of three biological replicates.

Table 2. MIC determination of *M. smegmatis* dKO (*ΔMSMEG_3069-70*).

Strain	Antibiotic	Tetracycline	Vancomycin	Rifabutin	Clofazimine	Novobiocin	Ofloxacin
WT	Median	0.5	256	4	0.5	32	0.5
	Range	(0.5)	(256–512)	(4–8)	(0.5)	(32)	(0.5)
dKO	Median	0.25	16	0.25	0.5	4	0.5
	Range	(0.25–0.5)	(8–16)	(0.125–0.5)	(0.5)	(4)	(0.5)
EV	Median	0.5	32	0.125	0.5	4	0.5
	Range	(0.25–0.5)	(32)	(0.125–0.25)	(0.5)	(4–16)	(0.5)
c. <i>mfs</i>	Median	0.5	64	1	0.5	8	0.5
	Range	(0.5)	(64–128)	(0.5–1)	(0.5)	(8)	(0.5)
c. <i>lprG</i>	Median	0.5	32	0.25	0.5	4	0.5
	Range	(0.25–0.5)	(16–32)	(0.25–0.5)	(0.5)	(4)	(0.5)
c. <i>lprG-mfs</i>	Median	0.5	512	4	0.5	16	0.5
	Range	(0.5–1)	(256–512)	(4–8)	(0.5–1)	(16–32)	(0.5)
c. <i>lprG-mfs</i>	Median	0.5	16	0.5	0.5	4	0.5
	Range	(0.5)	(16)	(0.25–0.5)	(0.5)	(4–8)	(0.5–1)
DtN	Range						

Complementation (c.) was carried out with the genes of the *lprG-mfs* operon from *M. smegmatis*. EV, empty vector control. DtN, MSMEG3069 D72N. MIC values correspond to µg ml⁻¹ of the respective antibiotics used. Shown are the median and range of three biological replicates.

The fusion protein was purified via the His-tag using the detergent β-DDM by immobilized metal ion affinity chromatography (IMAC) and GFP was cleaved off using HRV 3C protease. Subsequently, GFP and the His-tagged protease were removed by a reverse IMAC step, resulting in highly pure protein (Fig. 3A). Rv1410 was finally analyzed by size exclusion chromatography (SEC) and eluted as monodisperse peak at a retention volume corresponding to a Rv1410 monomer (Fig. 3B, red trace). Next, LprG was purified from the cytoplasm of *E. coli* in its non-acylated form as described previously (Drage *et al.*, 2010) and eluted at a retention volume corresponding to a monomer from SEC (Fig. 3B, green trace). To assess complex formation, Rv1410 and LprG were mixed and analyzed by SEC (Fig. 3B, black trace). However, we did not observe an early eluting peak, which would

correspond to the size of the Rv1410–LprG complex (Fig. 3B). Since the SEC method is only suited to detect high-affinity protein complexes, a SPR experiment was performed, which can detect affinities even in the micromolar range. To this end, Rv1410 was fused to an Avi-tag and purified for enzymatic biotinylation (Cull and Schatz, 2000) along with an Avi-tagged version of *E. coli* MdfA, which was used as negative control. SPR sensor chips were coated with biotinylated Rv1410 and MdfA, and purified LprG was injected as analyte at different concentrations. When injecting the highest three concentrations (22, 65 and 194 µM, respectively), LprG gave rise to a binding signal with Rv1410 (Fig. 3C). However, the same signal was also obtained with MdfA. Hence, the interaction is unspecific and presumably mediated through contacts of LprG with the detergent micelle of

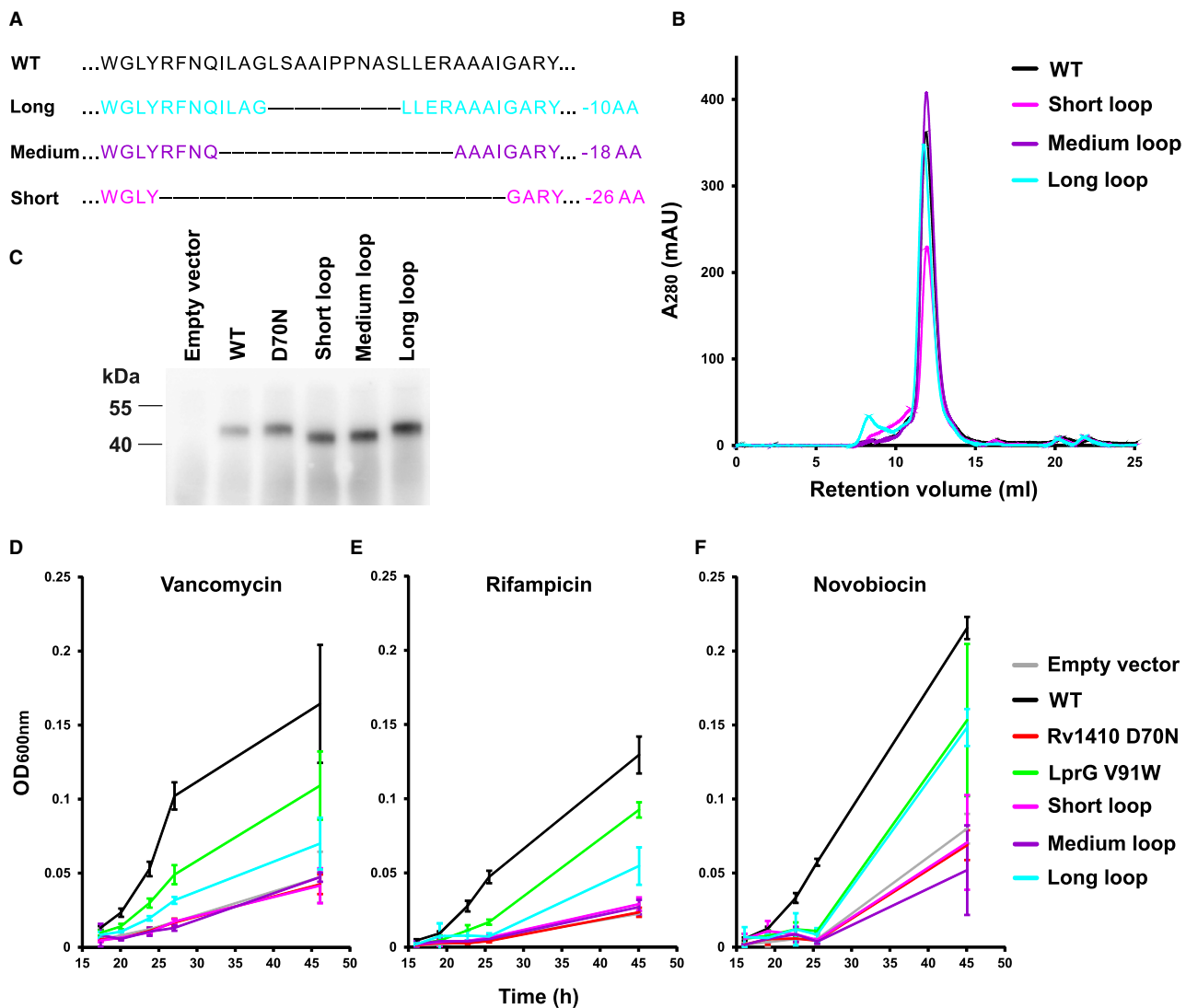


Fig. 2. Functional analysis of Rv1410's periplasmic loop.

A. Periplasmic loop sequence of wild-type Rv1410 (residues 430–463) and the three loop truncations.

B. Rv1410 with the respective loop truncations were purified from *E. coli* and separated by SEC. Purified wild-type Rv1410 served as reference.

C. Production levels of loop truncations of Rv1410 expressed in *M. smegmatis* dKO using complementation vector pFLAG were probed by Western blotting via a C-terminal 3xFLAG tag. *M. smegmatis* dKO harboring the empty pFLAG vector served as negative control.

M. smegmatis dKO expressing full-length Rv1410 (WT) and Rv1410 D70N served as positive control.

D–F. *M. smegmatis* dKO complemented with empty vector, the wild-type *lprG-rv1410* operon of *M. tuberculosis* and the operon containing mutations in *rv1410* (loop truncations and D70N) or *lprG* (V91W) was grown in the presence of vancomycin (D), rifampicin (E) and novobiocin (F). The growth curves are representative of three biological replicates and error bars denote the standard deviation of four to six technical replicates. [Colour figure can be viewed at wileyonlinelibrary.com]

purified Rv1410 and MdfA. In summary, our biophysical experiments revealed that Rv1410 and LprG do not form a complex, at least not outside of the membrane context.

Lack of *lprG-mfs* operon leads to increased drug influx

M. abscessus and *M. smegmatis* dKO mutants were clearly more susceptible toward vancomycin, a drug which acts in the periplasm as a cell wall synthesis

inhibitor (Perkins, 1969). Importantly, vancomycin does not need to enter the cytoplasm to inhibit cellular growth, and consequently, possible transport of vancomycin across the cytoplasmic membrane mediated by Rv1410 would not result in increased resistance toward this drug. This made us question the transporter's role as a drug efflux pump, which has been repeatedly proposed in the literature (Silva *et al.*, 2001; Ramon-Garcia *et al.*, 2009). We hypothesized that higher permeability of the

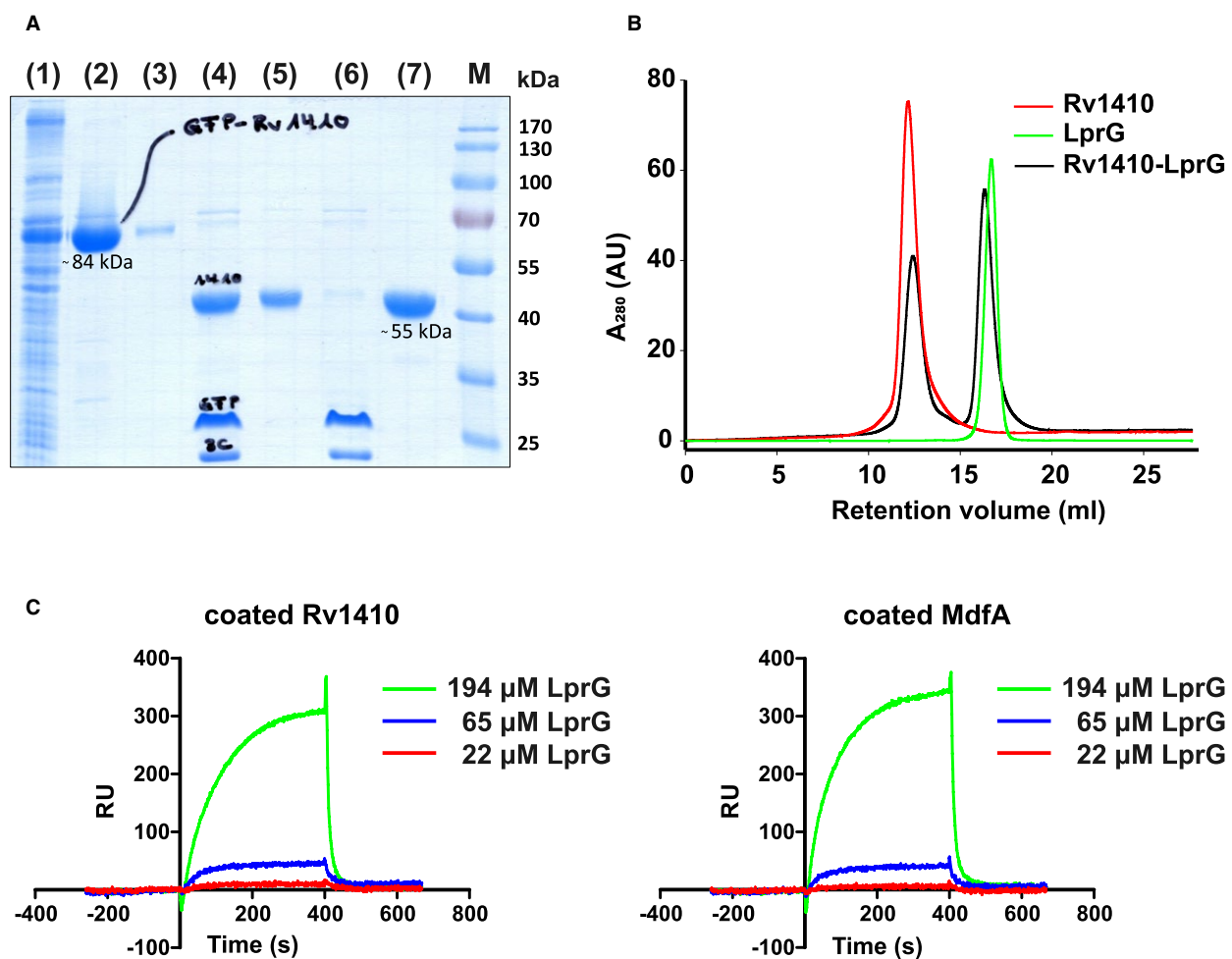


Fig. 3. Interaction studies of purified Rv1410 and LprG.

A. SDS-PAGE analysis monitoring the purification of Rv1410 expressed in *E. coli*. The following samples were loaded on the gel: (1) solubilized total membrane proteins, (2) elution from IMAC containing mainly His-tagged Rv1410-GFP fusion protein, (3) IMAC flow-through using wash buffer, (4) after cleavage with 3C protease, (5) flow-through of reverse IMAC after 3C cleavage containing tag-less Rv1410, (6) elution of reverse IMAC containing His-tagged GFP and His-tagged 3C protease, (7) highly pure Rv1410 after SEC.

B. Analytical SEC using purified Rv1410 alone (red trace), LprG alone (green trace) and Rv1410 and LprG mixed at a 1:5 molar ratio (black trace).

C. SPR analysis of Rv1410-LprG interaction. Rv1410 and control protein MdfA were immobilized and purified LprG served as analyte. [Colour figure can be viewed at wileyonlinelibrary.com]

cell envelope due to the lack of transport of LAMs, TAGs and presumably additional triacylated lipids to their correct locations could cause increased influx of drugs. We tested the hypotheses of drug efflux mediated by Rv1410 (Fig. 4A) and increased drug influx via a defective cell wall (Fig. 4B) by monitoring the accumulation of fluorescent substrates (ethidium, BCECF-AM, calcein-AM) in energized and de-energized cells.

As a positive control, we included the well-studied ethidium efflux pump LfrA of *M. smegmatis* (Sander *et al.*, 2000; Rodrigues *et al.*, 2011). Akin to Rv1410, LfrA is a DHA2 family MFS transporter with 14 transmembrane helices. In the presence of the proton-motive force (cells energized with glucose), we observed more accumulation of ethidium in the $\Delta lfrA$ strain compared

to the wild-type strain (Fig. 4C). However, when the cells were de-energized with the protonophore CCCP, a rise in the accumulation of ethidium was observed in both strains, resulting in comparable accumulation levels (Fig. 4C). Hence, in the absence of the proton-motive force, LfrA and other active transporters mediating ethidium efflux lose their ability to extrude ethidium and thus the wild-type strain displays a phenotype identical to the $\Delta lfrA$ strain.

Similar results would be expected if Rv1410 and LprG formed a drug efflux system. However, *M. smegmatis* dKO accumulated more BCECF and calcein than wild-type cells, regardless whether they were in an energized or de-energized state (Figs 4D and S2A). This observation suggests that the dKO strain exhibits an increased

dye permeability compared to wild-type cells. Hence, the data support the hypothesis that Rv1410 and LprG transport lipids required for the proper biogenesis of the

mycobacterial outer membrane, which remained unaffected by the addition of CCCP within the short time-frame of our experiments (Fig. 4B). Of note, BCECF and

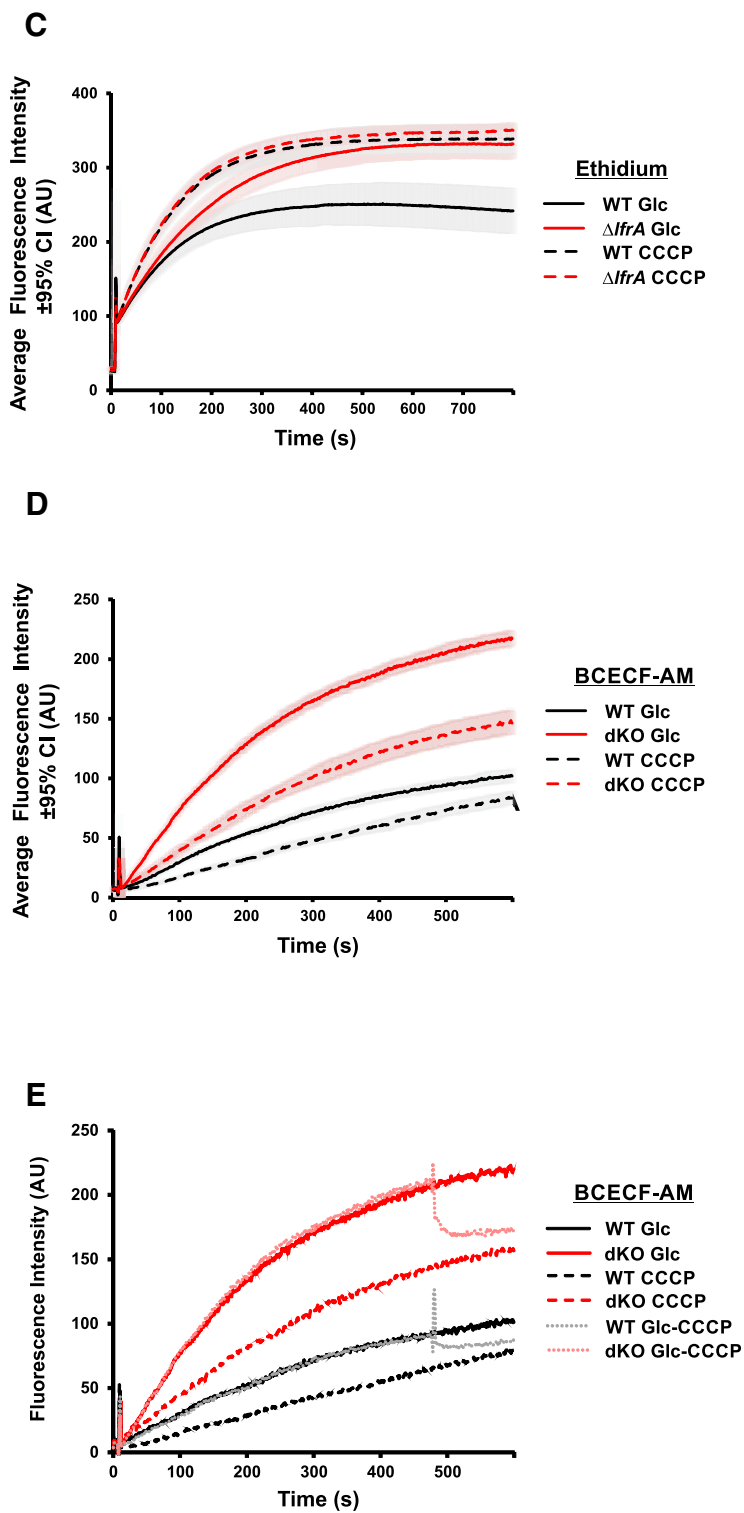
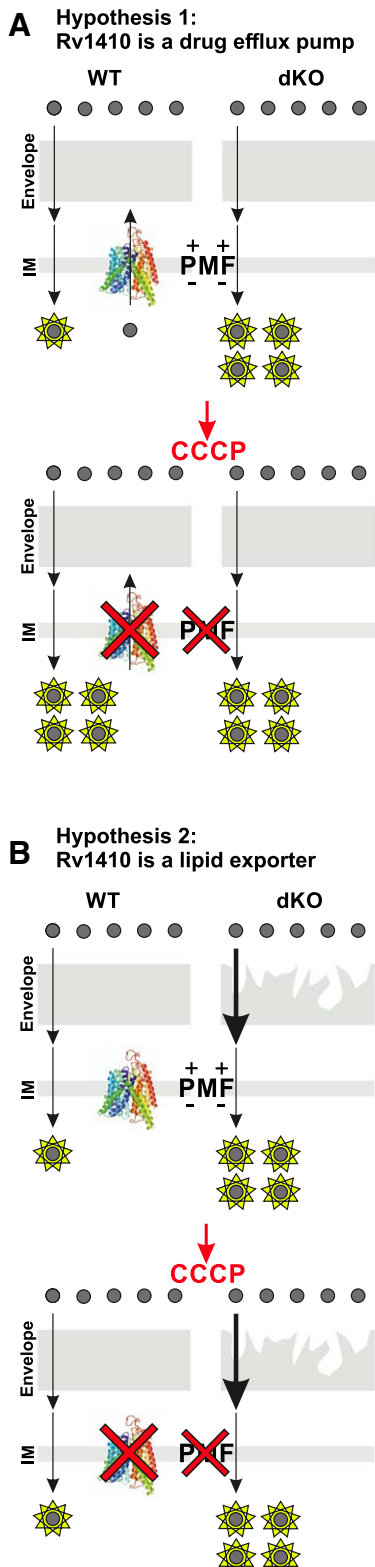


Fig. 4. Functional investigation of Rv1410 in *M. smegmatis*.

A and B. Two hypotheses predicting the functional outcome of a transport experiment assuming that Rv1410 is a drug efflux pump (A) or a lipid transporter (B). Gray circles represent non-fluorescent BCECF-AM, which is converted by intracellular esterases into fluorescent BCECF (yellow stars). Drug efflux pumps (here Rv1410) export BCECF-AM prior to esterase cleavage. Addition of CCCP disrupts the proton gradient across the inner membrane and thereby inactivates Rv1410. C. Ethidium transport in *M. smegmatis* mediated by the bona fide drug efflux pump LfrA, which follows the hypothesis shown in panel A. Ethidium was added to washed cells under energized (Glc) and de-energized (CCCP) conditions and ethidium uptake into the cell was monitored by fluorescence of ethidium intercalated into chromosomal DNA. D. BCECF-AM transport in *M. smegmatis* wild-type and dKO cells, which follows the hypothesis shown in panel B. Non-fluorescent BCECF-AM was added to washed cells under energized (Glc) and de-energized (CCCP) conditions and was converted into fluorescent BCECF by intracellular esterases. E. Traces of BCECF-AM uptake of energized (Glc) and de-energized (CCCP) cells are shown as in panel D. In addition, BCECF-AM uptake traces were recorded, in which CCCP was added to energized cells at time point 480 s (dotted lines, Glc-CCCP). CCCP addition leads to an immediate decrease of BCECF fluorescence, because the proton-motive force is eliminated resulting in a drop of intracellular pH. For the traces shown in panels C and D, average fluorescence intensities and 95% confidence intervals using a Student's *t* distribution were calculated from the data of six biological replicates. [Colour figure can be viewed at wileyonlinelibrary.com]

calcein fluorescence levels were in general lower under de-energized conditions due to the dependence of dye fluorescence on pH (Ozkan and Mutharasan, 2002; Boens *et al.*, 2006). When CCCP was added to cells energized with glucose, an immediate drop in fluorescence intensity was detected for BCECF (Fig. 4E) and calcein (Fig. S2B), respectively. This drop was caused by a sudden decrease of the cytoplasmic pH upon dissipation of the proton motive force and shows that substantial amounts of BCECF-AM and calceine-AM were converted into their fluorescent forms by intracellular esterases.

In conclusion, our data strongly support the hypothesis that Rv1410 and LprG contribute to the integrity and low permeability of the mycobacterial cell envelope by transporting important lipid constituents. Further, direct experimental evidence is provided suggesting that Rv1410 does not export fluorescent substrates out of the cell.

*Rv1410 does not mediate drug efflux in *L. lactis**

To further corroborate the lacking drug efflux activity of the MFS transporter, we expressed the *rv1410* gene of

M. tuberculosis in the Gram-positive bacterium *L. lactis*, which is a widely used model system to investigate drug efflux pumps (Seeger *et al.*, 2012; Hürliemann *et al.*, 2016). First, we confirmed that the bona fide efflux pumps LmrP and MdfA actively export the dyes ethidium, Hoechst 33342 and in case of LmrP BCECF-AM (Figs 5, S3A and B). Wild-type transporters were expressed along with the respective controls containing the inactivating DtoN mutation. BCECF-AM, ethidium or Hoechst 33342 was added to the washed cells in a glucose-containing buffer and the fluorescence arising from dye uptake was recorded. In this experimental setup, active dye efflux results in a slower rise of fluorescence. As expected, strong differences between bacteria expressing wild-type transporters and the respective DtoN mutants were observed for BCECF-AM (LmrP, Fig. 5B), ethidium (LmrP and MdfA, Fig. S3A) and Hoechst 33342 (LmrP, Fig. S3B), confirming that these proteins are drug efflux pumps. By contrast, under the same experimental conditions Rv1410 and Rv1410 D70N exhibited nearly identical fluorescence traces (Figs 5A, S3A and B), showing that Rv1410 appears to be unable to transport these dyes, which are common substrates for multidrug efflux pumps. Further, we determined the minimal

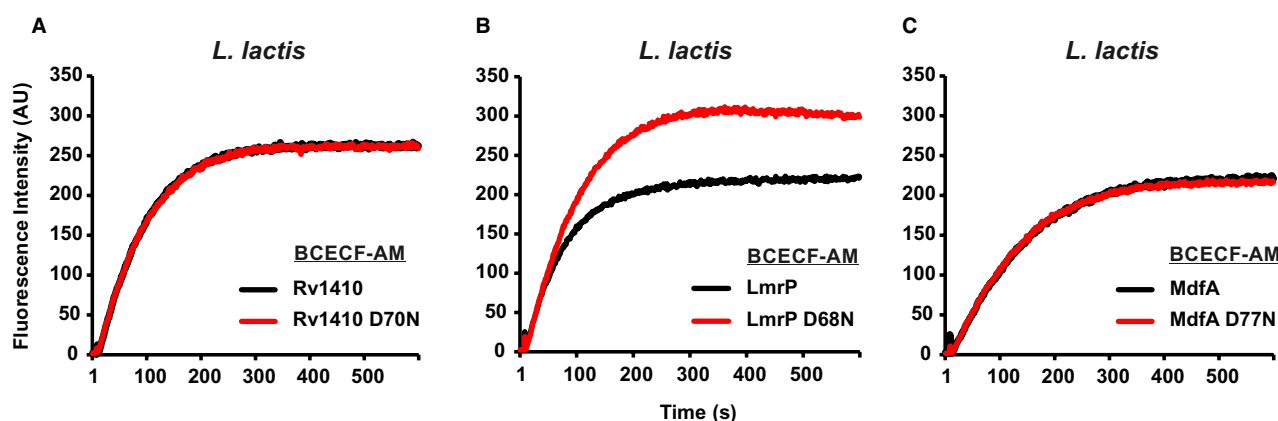


Fig. 5. BCECF-AM efflux mediated by Rv1410, LmrP and MdfA expressed in *L. lactis*. BCECF-AM was added to the washed *L. lactis* cells expressing wild-type Rv1410 (A), LmrP (B) and MdfA (C) or transporters carrying the corresponding DtoN mutations. BCECF accumulation in the cytosol was monitored by fluorescence. Only LmrP exhibits BCECF-AM efflux activity. [Colour figure can be viewed at wileyonlinelibrary.com]

inhibitory concentration for vancomycin, rifampicin and novobiocin using *L. lactis* cells expressing Rv1410, but did not find any difference between cells expressing the wild-type transporter versus the corresponding DtoN mutant (Fig. S3C). In order to assess expression levels, we fused GFP to the C-termini of the transporters and could show by in-gel fluorescence that all three transporters, including Rv1410, were well expressed (Fig. S3D). Of note, LmrP-GFP and MdfA-GFP were still capable of dye transport, whereas no efflux activity was observed for Rv1410-GFP (not shown). The lipid composition of *L. lactis* membranes is different from mycobacteria, which may cause incorrect folding and aggregation of the transporter. However, overexpressed Rv1410 purified from *L. lactis* membranes via its His-tag eluted as monodisperse peak from SEC at a retention volume corresponding to the size of a Rv1410 monomer, thereby excluding major folding and aggregation issues (Fig. S3E). In summary, Rv1410 is well expressed and properly folded in *L. lactis*, but lacks drug efflux activity.

M. smegmatis dKO cells are more rigid

We hypothesized that deletion of the *lprG-mfs* operon might also affect the mechanical properties of the cell surface and therefore investigated wild-type and dKO cells by AFM. Wild-type and dKO cells were mixed and imaged using correlated optical fluorescence microscopy (OFM) and AFM (Eskandarian *et al.*, 2017). Fluorescently labeled Wag31 was expressed in the wild-type cells to distinguish them from dKO cells (Santi *et al.*, 2013). Control experiments in which the dKO mutant was labeled with fluorescent Wag31 excluded the possibility that fluorescent protein expression affected the experimental outcome. The mean surface rigidity, represented as the elastic modulus, was calculated for wild-type and dKO cells from images obtained by AFM (Fig. 6A and B). Interestingly, the mean surface rigidity of the dKO mutant was found to be significantly higher than in wild-type cells (Fig. 6C).

M. smegmatis dKO has a cell separation defect

We used transmission electron microscopy (TEM) to investigate whether lack of the *lprG-mfs* operon influences cellular morphology. Interestingly, we noticed a cell separation defect as manifested by long cell chains divided by multiple septa (Fig. 7A), which appeared to be more prevalent in *M. smegmatis* dKO. In order to quantify this defect, we used fluorescence microscopy to analyze mycobacterial cells that were stained with the membrane dye SynaptoRed. In addition, the cells expressed the Wag31–GFP fusion protein, which localizes to septa formed during cell division and remains

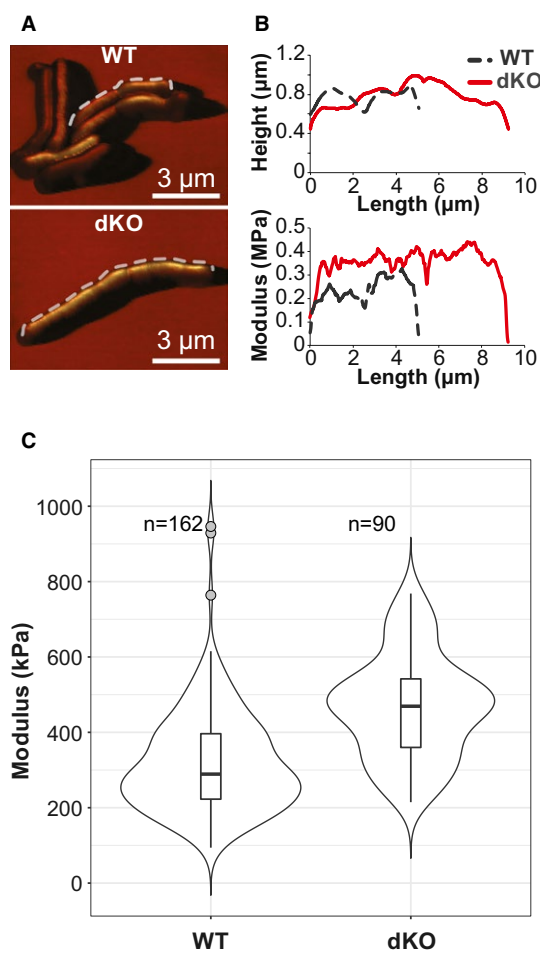


Fig. 6. Analysis of cell surface rigidity of *M. smegmatis* by correlated optical fluorescence and AFM.

A. AFM images of representative wild-type and dKO cells are depicted in 3D with the AFM stiffness (DMT modulus) image overlaid as a skin on top of the AFM height image. Cell profiles were harvested from AFM images by drawing a segmented line along the midline of the cell length along which the AFM height (B, top panel) as well as the DMT modulus providing a measure for cell surface rigidity (B, bottom panel) were plotted.
C. Violin plot of the average DMT modulus of wild-type ($n = 162$) and dKO ($n = 90$) cells. The horizontal black bars represent the median DMT modulus, the boxes correspond to the interquartile ranges, the straight vertical lines contain all data points except for the outliers marked as dots. Two-sided Wilcoxon rank sum test identified statistically significant location shift between WT and dKO samples with a p -value of 1.02×10^{-14} . [Colour figure can be viewed at wileyonlinelibrary.com]

attached to the poles (Santi *et al.*, 2013) (Fig. 7B). Overall, 1105 cell chains were counted. Because the experiments and data analysis were conducted blinded, the number of dKO strain and wild-type strain differed by a factor of around 2 (Fig. 7C). Upon data normalization, we observed 3 times more chains consisting of three or more cells in the dKO strain compared to the wild-type strain (Fig. 7D). Pearson's χ^2 test showed significant difference in the distribution of the cell chains of different lengths between wild-type and dKO strains

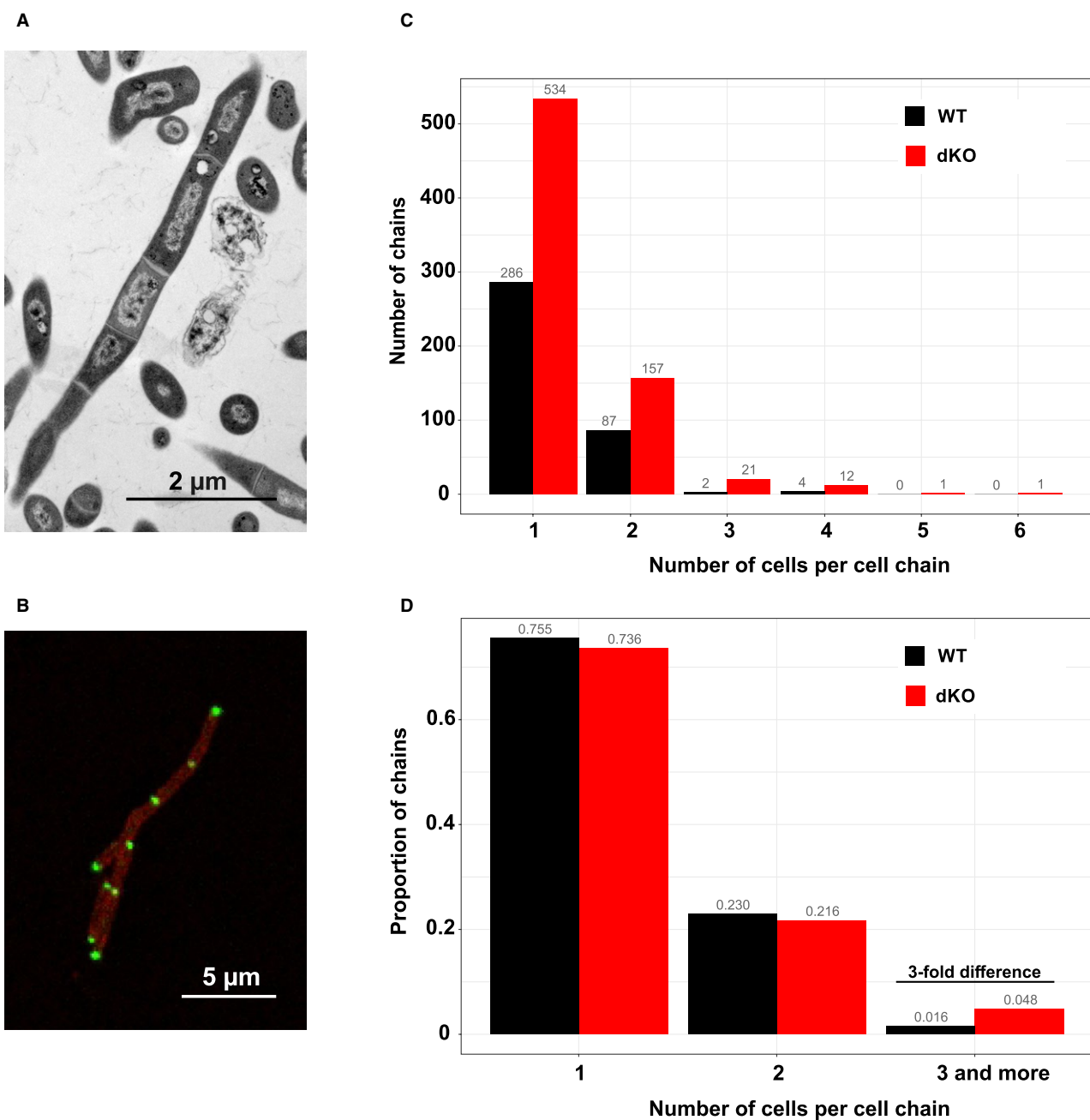


Fig. 7. *M. smegmatis* cells lacking the *lprG-mfs* operon have a cell separation defect.

- A. Transmission electron microscopy image of a *M. smegmatis* dKO cell chain divided by multiple septa.
- B. Exemplary 3D fluorescence microscopy image of *M. smegmatis* dKO cells stained with SynaptoRed membrane dye and expressing the Wag31-GFP fusion proteins localizing at septa and cell poles. Such images were used to quantify the cell separation defect.
- C. Distribution of the number of cells per chain of wild-type ($n = 379$) and dKO ($n = 726$) cells.
- D. Normalized distribution of the number of cells per chain of wild-type and dKO cells, in which >3 cells per chain are summarized in one bar. Pearson's χ^2 test showed significant difference in the distribution of the cell chains ($\chi^2 = 7.3571$, $df = 2$, p -value = 0.02526). [Colour figure can be viewed at [wileyonlinelibrary.com](#)]

($\chi^2 = 7.3571$, $df = 2$, p -value = 0.02526). These results suggest the presence of a cell separation defect after the cell division event. The extent of the cell separation defect was probably underestimated, because long cell chains are more likely to become entangled in cell clusters which were excluded from data analysis.

Discussion

Rv1410 and its operon partner LprG have been the subject of numerous studies in past years. Whereas LprG's role is to bind triacylated lipids such as LAMs, PIMs and TAGs, Rv1410 was proposed to possess a

dual function, namely drug efflux as well as lipid transport (Farrow and Rubin, 2008; Ramon-Garcia *et al.*, 2009). In this work, we observed that deletion of the *lprG-mfs* operon in *M. smegmatis* and *M. abscessus* resulted in a marked increase of vancomycin, rifampicin/rifabutin and novobiocin susceptibility, a result that is in full agreement with a previous study on *M. bovis* BCG (Ramon-Garcia *et al.*, 2009). While rifampicin/rifabutin and novobiocin target intracellular proteins, vancomycin has its target in the periplasm. Importantly, periplasmic vancomycin concentrations solely depend on the diffusion across the outer membrane, and consequently, Rv1410-mediated vancomycin export across the inner membrane cannot account for vancomycin resistance. Rather, the activity of Rv1410 appears to be required for the correct assembly of the mycobacterial outer membrane. In further support of this notion, cells lacking the operon were found to accumulate more BCECF and calcein dyes, irrespective whether they were in an energized or de-energized state. Hence, active dye efflux mediated by Rv1410, which depends on the proton-motive force, cannot explain this observation. Finally, Rv1410 expressed in *L. lactis* did not exhibit efflux activity toward BCECF-AM, ethidium and Hoechst 33342, nor did it confer resistance toward vancomycin, rifampicin or novobiocin, despite of the fact that the transporter was expressed at high levels and well folded.

We show in this work that Rv1410 critically depends on the proton-motive force, because substitution of a conserved aspartate by asparagine (Dtn mutation), a residue coupling substrate transport to the influx of protons, completely abrogated Rv1410's capacity to confer resistance toward all drugs tested, including the periplasmic drug vancomycin. Hence, inclusion of protonophores in the growth medium does not only inhibit the potential drug efflux activity of Rv1410, but also its lipid transport activity and consequently the correct assembly of the outer membrane during the long growth period. Therefore, previous experiments performed in the presence of sub-inhibitory CCCP concentrations from which it was concluded that Rv1410 is an efflux pump for rifampicin and novobiocin are likely ambiguous (Ramon-Garcia *et al.*, 2009). In order to differentiate between drug and lipid transport activity mediated by Rv1410, we chose an experimental design in which we added CCCP to washed cells shortly prior to the addition of the dyes BCECF-AM or calcein-AM. Thereby we avoided defects of the outer membrane and were able to truly distinguish drug influx from drug efflux. These experiments clearly revealed that increased BCECF and calcein accumulation in mutant cells is solely attributable to increased influx, unequivocally suggesting an outer membrane defect resulting in increased dye permeability. It is interesting to note that certain mutations affecting the

lipopolysaccharide (LPS) biosynthesis of Gram-negative bacteria exhibit drug susceptibility profiles that are very similar to the *lprG-mfs* operon deletion mutants observed here and in *M. bovis* BCG (Ramon-Garcia *et al.*, 2009). Most prominent in this context are the *lpxC* (originally called *envA*) mutations in *E. coli*, which are defective in Lipid A biosynthesis resulting in periplasmic leakage of proteins and higher susceptibility toward larger drugs including rifampicin, novobiocin and vancomycin, that cannot be transported through outer membrane porins (Young and Silver, 1991; Young *et al.*, 1995; Nikaido, 2005).

In addition to the increased outer membrane permeability, we observed a cell separation defect in *M. smegmatis* lacking the operon, as manifested by long chains of cells separated by already formed septa. Interestingly, such chain-forming phenotypes displaying septation and cell separation defects have been described for several Gram-negative bacterial mutants containing a defective outer membrane (Normark *et al.*, 1969; Weigand *et al.*, 1976; Stanley *et al.*, 2001).

Using state-of-the-art AFM, we could demonstrate that the cell surface of the deletion mutants is significantly more rigid. At first sight, a connection between increased membrane stiffness and higher permeability appears counterintuitive. Indeed, AFM studies on isolated membrane vesicles with defined lipid compositions revealed that membranes of higher rigidity are less permeable for calcein (Takechi-Haraya *et al.*, 2017). However, lipid vesicles are several orders of magnitude softer than the complex mycobacterial outer membrane, suggesting that the physical principle underlying membrane permeability differs among them. Interestingly, an *E. coli* mutant unable to incorporate unsaturated fatty acid chains into lipid A became hypersusceptible toward vancomycin and rifampicin at 12°C, but not at 30°C, indicating that large drugs can enter the periplasm through a stiffened outer membrane (Vorachek-Warren *et al.*, 2002). Our results suggest that lack of the *lprG-mfs* operon results in a rigidified mycobacterial outer membrane, which might contain imperfections and 'cracks' through which large drugs and dyes gain access to the periplasm.

The aggregated data on Rv1410 and LprG as outlined in previous works and here clearly suggest that these proteins form a tandem responsible for the transport of triacylated lipids for the correct biogenesis of the outer mycobacterial membrane (Fig. 8). But how do they work in concert? In this study, we showed that the MFS transporter plays the dominant role of the duo, because its expression as solitary protein in *M. smegmatis* and in particular in *M. abscessus* to a large degree reversed drug susceptibility. It is thus conceivable that Rv1410 and its mycobacterial orthologues can cooperate with lipo-proteins other than LprG, which may partially substitute

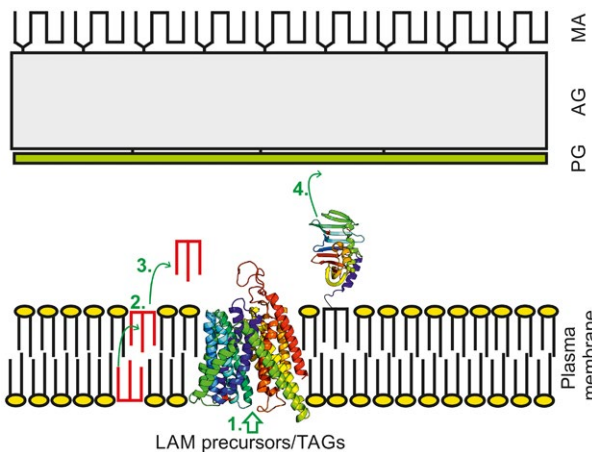


Fig. 8. Hypothetical mechanisms of lipid transport mediated by Rv1410 and LprG. 1. Rv1410 may transport TAGs (red) and LAM precursors across the plasma membrane. 2. Rv1410 may flip TAGs from the inner to the outer leaflet of the plasma membrane. 3. Rv1410 may extract TAGs from the outer leaflet of the plasma membrane and deliver them to LprG. 4. Rv1410 may extract the lipid anchor of LprG from the outer leaflet to facilitate LprG-mediated TAG transport to the outer membrane. PG: peptidoglycan, AG: arabinogalactan, MA: mycolic acids. [Colour figure can be viewed at wileyonlinelibrary.com]

LprG's function. In support of this view, we observed that purified Rv1410 and LprG do not physically interact with each other, at least not via a classical protein-protein interaction that can be observed outside of the membrane context. LprG was proposed to be responsible for the shuttling of triacylated lipids across lipid membranes, as was shown in biochemical *in vitro* experiments (Martinot *et al.*, 2016). In the same study, the role of Rv1410 was proposed to flip TAGs and presumably other triacylated lipids across the inner membrane (Martinot *et al.*, 2016). However, functional evidence supporting this hypothesis is currently lacking. Given the fact that *rv1410* and its orthologues are nonessential genes, it is unlikely that this MFS transporter is the only protein responsible for such a crucial transport activity. In analogy to the *E. coli* Lpt pathway of LPS transport, in which the ABC transporter LptB₂FG extracts LPS from the outer leaflet of the cytoplasmic membrane in an ATP-dependent fashion to be transferred to periplasmic LPS shuttling proteins (Okuda *et al.*, 2016), Rv1410 may be required to extract TAGs, LAMs and other triacylated lipids from the outer leaflet of the inner mycobacterial membrane and deliver them to LprG (Fig. 8). In such a model, Rv1410's role is to charge LprG with a substrate. The conspicuous periplasmic loop between TM11 and TM12 may play a role in transferring lipids to LprG, because its deletion abrogates the function of the operon. It should be noted that LprG is a lipoprotein, which is anchored in the outer leaflet of the cytoplasmic membrane via three acyl-chains. It is therefore also imaginable that Rv1410's role is to extract LprG from the

membrane to send it on its journey across the periplasm to the outer membrane to deliver its cargo lipids. In *E. coli*, the ABC transporter LolCDE powers the extraction of the lipoprotein from the inner membrane using the energy of ATP and delivers it to the periplasmic shuttling protein LolA (Yakushi *et al.*, 2000). Currently, these possible mechanisms of Rv1410 are purely speculative and detailed biochemical *in vitro* studies are needed to further address the important question of how Rv1410 and LprG work in concert to shuttle lipids from the inner to the outer mycobacterial membrane.

Experimental procedures

Bacterial strains and growth conditions

Mycobacterium smegmatis mc² 155 and *Mycobacterium abscessus* (ATCC19977T) were used in this study. Mycobacteria were grown at 37°C in liquid Middlebrook 7H9 medium containing 0.05% Tween 80 or on solid Middlebrook 7H10 medium supplemented with OADC containing 4.5 ml L⁻¹ glycerin. *Escherichia coli* MC1061, the strain used during cloning and for heterologous protein expression, was grown in lysogeny broth medium (LB) or Terrific broth medium (TB) at 37°C or 25°C respectively. *Lactococcus lactis* Δ*lmrA* Δ*lmrCD* (Venter *et al.*, 2008) was grown in M17 medium supplemented with 0.5% glucose (GM17) at 30°C without shaking (Hürlimann *et al.*, 2016). Where required, the medium was supplemented with the following amounts of antibiotics: 100 µg ml⁻¹ of ampicillin (Amp¹⁰⁰), 5 or 25 µg ml⁻¹ of chloramphenicol (Cm⁵/Cm²⁵) for *L. lactis* and *E. coli*, respectively, 25 µg ml⁻¹ of apramycin (Apr²⁵) for *M. smegmatis* or 50 µg ml⁻¹ apramycin (Apr⁵⁰) for *E. coli* and *M. abscessus*, and 32 µg ml⁻¹ isoniazid for *M. abscessus*.

Gene deletion of lprG-mfs (MSMEG_3069-70) and IfrA (MSMEG_6225) in *M. smegmatis*

Gene deletions in *M. smegmatis* mc² 155 were generated by a two-step recombination approach. The flanking regions of the respective genetic loci were amplified by PCR from genomic DNA (gDNA) using primers listed in Table S1. Both fragments were purified via agarose gel, cut with BspQI, cloned in one step into pINIT (Cm²⁵) using fragment exchange (FX) cloning (Geertsma and Dutzler, 2011). After sequencing, the fragments were cut from pINIT and cloned into the mycobacterial suicide vector pKO, which was propagated in *E. coli* using Apr⁵⁰ (Arnold *et al.*, 2018). For the first recombination step, the pKO vectors carrying the flanking regions were transformed into *M. smegmatis* by electroporation and plated on 7H10 plates containing Apr²⁵. Colonies appeared after 3–4 days incubation and were grown in 5 ml liquid 7H9 (Apr²⁵) for 2–3 days. gDNA was isolated (GenElute™ Bacterial Genomic DNA Kit, Sigma) and was analyzed by PCR for 5' and/or 3' integration. PCR-positive clones were grown in liquid 7H9 medium devoid of apramycin for 2–3 days and 1 µl was plated on 7H9 plates containing 0.5% 2-Deoxy-Galactose (2-DOG) and 10% sucrose for counterselection. Colonies were resuspended in 10 µl

dH₂O and screened by PCR to differentiate between gene deletions or wild-type revertants. gDNA of identified gene deletion mutants was isolated to confirm gene deletions by PCR and the strains were tested for susceptibility toward apramycin.

Gene deletion of lprG-mfs (MAB_2806-07) in *M. abscessus* ATCC19977T

To construct the gene deletion mutant, gene deletion vector pSE-arp-katG-ΔlprG-ΔMAB_2807 was generated. To this end, a 1526 bp fragment upstream of the target genes was amplified by PCR with the primers MAB_2806/07_5'_for and MAB_2806/07_5'_rev and a 1467 bp fragment downstream of the genes with the primers MAB_2806/07_3'_for and MAB_2806/07_3'_rev (primer sequences are found in Table S1). The primers were appended with PscI, XbaI or HindIII recognition sites (underlined in Table S1). The PCR fragments were first cloned into pGEM-T easy (Promega), from which they were cut using the corresponding restriction enzymes and successively cloned into the linearized pSE-arp-katG vector to result in the final gene deletion suicide vector pSE-arp-katG-ΔlprG-ΔMAB_2807. The vector was transformed into *M. abscessus* ATCC 19977T as previously described (Rominski et al., 2017). Putative single cross-over colonies were selected on Apr⁵⁰ and confirmed by Southern blotting. Double cross-over recombinants were subsequently selected on isoniazid (32 µg ml⁻¹) and confirmed by Southern blotting (Rominski et al., 2017).

Gene cloning into the FX cloning initial vector pINIT

All expression constructs were generated using the FX cloning method (Geertsma and Dutzler, 2011), which was recently expanded with a vector series suitable for mycobacteria (Arnold et al., 2018). As a first step, the open reading frames of interest were cloned into an initial vector (pINIT, Cm²⁵), sequenced and then used for sub-cloning by fragment exchange into the required destination vectors (see below). Using primers specified in Table S2, Q5 High-Fidelity DNA polymerase (NEB) and if not stated otherwise genomic DNA (gDNA) as template, the following genes were amplified. (1) The *lprG-mfs* operons and its single genes of *M. smegmatis* mc² 155, *M. abscessus* ATCC19977T (gDNA) and *M. tuberculosis* H37Rv (bacmid library as PCR template (Brosch et al., 1998)); (2) a truncated version of *lprG* called *lprG_trunc* without signal sequence and lipobox as described previously (Drage et al., 2010) from *M. tuberculosis* for cytoplasmic expression; (3) *lmrP* from *L. lactis*; (4) *mdfA* from *E. coli*. PCR products were purified via agarose gel, cut with BspQI and cloned into pINIT using chemically competent *E. coli* MC1061 cells. The ORFs in the resulting pINIT constructs were completely sequenced. Mutations in the lipoprotein or the MFS transporter genes (pINIT) were introduced using the QuikChange site-directed mutagenesis protocol (primers listed in Table S3). Rv1410 loop truncations were generated by PCR amplification of pINIT_rv1410-11 (for complementation) or pINIT_rv1410 (for protein expression and purification) using primers listed in Table S3, resulting in a large blunt-ended PCR product lacking

the nucleotides encoding for the loop. The PCR products were treated with DpnI (NEB), ligated with T4 ligase (Thermo Scientific), and transformed into *E. coli* MC1061. Loop truncations were confirmed by sequencing.

Cloning of transporters for expression in *L. lactis*

Transporters genes encoding for Rv1410, LmrP and MdfA and the corresponding DtoN mutants were sub-cloned from the pINIT constructs into *E. coli* vectors pREXC3H and pREXC3GH (Geertsma and Dutzler, 2011) and from there via vector-backbone exchange (VBEx) cloning into the *L. lactis* expression vector pNZ8048, which is under the control of the nisin-inducible promoter (Geertsma and Poolman, 2007). For transport experiments, the transporters were cloned into pNZ8048 via vector pREXC3H, resulting in a fusion of a HRV 3C protease cleavage site and a His₁₀-tag to the C-termini of the proteins. For protein detection and purification, cloning into pNZ8048 via pREXC3GH was performed, which adds a 3C site, a GFP and His₁₀-tag to the C-terminus of the expressed transporters.

Construction of mycobacterial complementation vectors

For complementation, the integrative mycobacterial vector pFLAG was used (Arnold et al., 2018). It contains a constitutive *tet*-promoter and adds a 3xFLAG sequence to the C-terminus of the cloned genes for detection by Western blotting. The *lprG-mfs* operons, its single genes as well as site directed mutants and loop truncation mutants were sub-cloned from pINIT (see above) into pFLAG and propagated in *E. coli* (Apr⁵⁰). The resulting pFLAG expression vectors were integrated into the genome of *M. smegmatis* Δ*lprG-mfs* (ΔMSMEG_3069-70) by co-electroporation with suicide plasmid pMA_Int harboring the L5 bacteriophage integrase (Arnold et al., 2018). Cells were plated on 7H10 (Apr²⁵) and colonies were picked and grown in 7H9 (Apr²⁵). Of note, because pFLAG does not contain the integrase gene, the integration is stable also in the absence of the selection marker apramycin (Springer et al., 2001).

Western blotting to detect loop mutant production in *M. smegmatis*

Cultures of *M. smegmatis* dKO complemented with empty vector pFLAG, and pFLAG harboring Rv1410, Rv1410 D70N, or the three Rv1410 loop truncation mutants were grown into stationary phase. The OD₆₀₀ of the cultures were adjusted to an identical value and harvested. The cell pellets were resuspended in 500 µl 20 mM Tris/HCl pH 8, 200 mM NaCl, a spatula tip of acid-washed glass beads ≤106 µm (Sigma) was added, and then the cells were lysed with a FastPrep-24 Classic cell lysis machine (MP Biomedicals) for 3 cycles of 60 s at 6 m s⁻¹. The lysate was spun 5 min at 8,000 rpm at 4°C with a F-45-30-11 rotor (Eppendorf) to pellet glass beads and cell debris. 100 µl of supernatant were mixed with 25 µl of 5x SDS loading dye (120 mM Tris/HCl pH 6.8, 50% glycerol, 100 mM DTT, 2% SDS (w/v), 0.1% bromophenol blue (w/v)), of which 10 µl were loaded

on a 4%–20% SDS-PAGE gel (ExpressPlusTM PAGE gel, Genscript). Separated proteins were transferred to a membrane (Immobilon-PSQ, Merck) by soaking the gel and membrane in transfer buffer (2.9 g glycine, 5.8 g Tris, 0.1% SDS (w/v) and 20% methanol (v/v) in 1 liter), and transferring with a Trans-Blot[®] SD Semi-Dry Electrophoretic Transfer Cell (BIO-RAD) for 1 h at 12 V. Then the membrane was blocked in PBS buffer containing 5% (w/v) milk powder and 0.05% (v/v) Tween20 for 1 h at RT, incubated in blocking buffer with anti-FLAG antibody (Sigma, F3165) diluted 1:10,000 (v/v) for 1 h at RT while rotating, and washed 3x with washing buffer (PBS containing 0.05% (v/v) Tween20). The membrane was incubated with α -mouse-HRP antibody (Sigma, A5278) diluted 1:30,000 (v/v) for 1 h at RT, washed again 3 times with washing buffer. The proteins were visualized by adding Immobilon Western Chemiluminescent HRP Substrate (Merck) and measuring chemiluminescence using ImageQuant LAS 4000 (GE Healthcare).

Construction of E. coli vectors for the expression of Rv1410, LprG_trunc, Rv1410-AviC and MdfA_AviC

By subcloning genes from pINIT (see above), the following arabinose-inducible pBX-vectors (Geertsma and Dutzler, 2011) for protein expression and purification were constructed: (1) pBXC3H_LprG_trunc encoding for LprG_trunc (no signal sequence and lipobox, as described in (Drage *et al.*, 2010))/3C protease-cleavage site/His₁₀-tag, (2) pBXC3GH_Rv1410 encoding for Rv1410/3C/GFP/His₁₀-tag, (3) pBXCA3GH_Rv1410 encoding for Rv1410/Avi-tag/3C/GFP/His₁₀-tag and (4) pBXCA3GH_MdfA encoding for MdfA/Avi-tag/3C/GFP/His₁₀-tag. The latter two constructs contain an Avi-tag for enzymatic biotinylation after protease cleavage (Bukowska *et al.*, 2015).

Expression and purification of M. tuberculosis Rv1410 and LprG_trunc

E. coli MC1061 precultures harboring pBXC3GH_Rv1410 or pBXC3H_LprG_trunc were directly inoculated from glycerol stocks in LB, Amp¹⁰⁰ and grown at 37°C overnight. The precultures were diluted 1:40 (v/v) into fresh expression medium (TB, Amp¹⁰⁰) and grown for 2 h at 37°C and an additional hour at 25°C before induction of protein expression with 0.002% L-arabinose overnight. Cells were harvested for 20 min at 6,000 rpm in a Fiberlite F10-4x1000 LEX centrifuge rotor at 4°C. Membranes were prepared by disrupting the cells with a Microfluidizer (Microfluidics) at 30 kpsi in 20 mM Tris/HCl pH 8.0, 200 mM NaCl supplemented with 3 mM MgSO₄ and traces of DNasel on ice. In case of Rv1410, unbroken cells and cell debris were removed by centrifugation for 30 min at 8,000 rpm in a Sorvall SLA-1500 rotor at 4°C. Membranes were collected in a Beckman Coulter ultracentrifuge using a Beckman Ti45 rotor at 38,000 rpm for 1 h at 4°C and resuspended in TBS (pH 7.5) containing 10% glycerol. Membranes were solubilized for 2 h using 1% β -DDM (w/v); insolubilized material was removed by ultracentrifugation. The supernatant was loaded on Ni²⁺-NTA columns, washed with 50 mM imidazole (pH 7.5), 200 mM NaCl, 10% glycerol,

0.03% β -DDM and eluted with 200 mM imidazole (pH 7.5), 200 mM NaCl, 10% glycerol, 0.03% β -DDM. In order to remove the C-terminally attached GFP/His₁₀-Tag the buffer of the protein preparation was first exchanged (20 mM Tris/HCl pH 7.4, 150 mM NaCl, 0.03% β -DDM) via a PD-10 desalting column. In a second step 3C protease cleavage was performed overnight. In case of LprG_trunc, unbroken cells and cell debris were removed by centrifugation for 30 min at 15,000 rpm in a Beckman Coulter ultracentrifuge at 4°C using a Beckman Ti45 rotor. The supernatant was loaded on Ni²⁺-NTA columns, washed with 50 mM imidazole (pH 7.5), 200 mM NaCl, 10% glycerol and eluted with 200 mM imidazole (pH 7.5), 200 mM NaCl, 10% glycerol. In order to remove the attached C-terminal His₁₀-tag and get rid of the imidazole the affinity-purified protein was dialyzed against 20 mM Tris/HCl pH 7.4, 150 mM NaCl and simultaneously cleaved by 3C protease. Finally, cleaved Rv1410 and LprG_trunc were again loaded on a Ni²⁺-NTA column to remove GFP/His₁₀-tag and the His-tagged 3C protease and were separated by size exclusion chromatography (SEC, Superdex 200 10/300 GL) in 20 mM Tris/HCl pH 7.4, 150 mM NaCl, 0.03% β -DDM. Protein concentrations were determined by measuring A₂₈₀ using NanoDrop 2000c.

Expression and purification of biotinylated Rv1410_AviC and MdfA_AviC containing a C-terminal Avi-tag

The purification of Avi-tagged versions of Rv1410 (Rv1410_AviC) and MdfA (MdfA_AviC) was performed the same way as described above for Rv1410 with the exception that an additional biotinylation step was introduced between the Ni²⁺-NTA purification and the buffer exchange using a PD-10 column. The eluted protein from the Ni²⁺-NTA column was concentrated to approximately 250 μ l. A final concentration of 5 mM ATP, 10 mM MgOAc, a 2-fold excess of biotin over the Avi-tag concentration, 16 μ g ml⁻¹ BirA, 200 mM NaCl and 10% glycerol was added to the protein to reach a final volume of 2.5 ml. The biotinylation reaction was incubated for 16–18 h at 4°C. After this step the standard purification described above was performed.

Analytical size exclusion chromatography (SEC) to investigate Rv1410-LprG interaction

The main elution fractions of the monodisperse SEC peaks of the lipoprotein LprG_trunc and Rv1410 were first separated individually by SEC (Superdex 200 10/300 GL) in 20 mM Tris/HCl pH 7.4, 150 mM NaCl, 0.03% β -DDM. Then, the collected fractions of the main peak of each protein were pooled and the two proteins were mixed together. LprG_trunc was added at a fivefold excess over the transporter Rv1410, incubated for 15 min on ice and analyzed by SEC.

Surface plasmon resonance

The affinity of the MFS transporter Rv1410 to the lipoprotein LprG_trunc was assessed by SPR analysis on a ProteOn XPR36 protein interaction array system

(Bio-Rad). Biotinylated Rv1410-AviC (500 RU) and as a control biotinylated MdfA-AviC (500 RU) was immobilized on a NeutrAvidin coated NLC sensor chip in SPR buffer (20 mM Tris/HCl (pH 7.4), 150 mM NaCl, 0.05% Tween-20). LprG_{trunc} was injected at six different concentrations (0, 2.4, 7.2, 21.6, 64.8, 194.4 µM). SPR measurements were performed with 400 s contact time followed by 280 s dissociation time at a flow rate of 30 µl min⁻¹. Given the fact that LprG_{trunc} interacted unspecifically with MdfA at the highest analyte concentrations, the data were not further quantified.

*Expression tests of GFP-fused transporters in *L. lactis* and purification of Rv1410-GFP from *L. lactis**

L. lactis NZ9000 ΔImrA ΔImrCD cells (Venter *et al.*, 2008) harboring plasmids encoding Rv1410-GFP, LmrP-GFP or MdfA-GFP were grown in GM17 Cm⁵ at 30°C. Expression was induced at an OD₆₀₀ of 0.4–0.6 with nisin (culture supernatant of *L. lactis* NZ9700) for 2 h (1:1,000 (v/v)). 4 ml of cells were harvested in 2 ml tubes and resuspended in 350 µl 20 mM Tris/HCl pH 8, 200 mM NaCl. A spatula tip of acid-washed glass beads ≤106 µm (Sigma) was added and the cells were subsequently lysed with a FastPrep-24 Classic cell lysis machine (MP Biomedicals) for 3 cycles of 60 s at a force of 6 m s⁻¹. The lysate was spun 15 min at 14,000 rpm at 4°C with a F-45-30-15 rotor (Eppendorf) to pellet glass beads and cell debris. The supernatant containing membrane vesicles was pelleted by ultracentrifugation and the membrane pellet was dissolved in 10 µl of 5x SDS loading dye (120 mM Tris/HCl pH 6.8, 50% glycerol, 100 mM DTT, 2% SDS (w/v), 0.1% bromophenol blue (w/v)), and separated by a 10% SDS-PAGE gel. The GFP-fusions were detected by in gel fluorescence with an ImageQuant LAS 4000 instrument (GE Healthcare).

For the purification of Rv1410, Rv1410-GFP was expressed in *L. lactis* NZ9000 ΔImrA ΔImrCD as described above using 4 liters of medium. The cell pellet was resuspended in PBS containing 15 mM K-EDTA and protease inhibitor. The cells were then disrupted using a Benchtop Microfluidizer M110PS (Microfluidics) 3 times at 30 kpsi. The cell lysate was centrifuged at 8,000 rpm at 4°C for 10 min (Centrifuge 5804R, rotor: A-4-44 by Eppendorf) and the supernatant was incubated with 20 mM MgCl₂ and DNase I (1:1,000 v/v) on ice for 30 min. Subsequently, ultracentrifugation was performed at 42,000 rpm and 4°C for 1 h using a Beckman Ti45 rotor. The pelleted membrane was resuspended in TBS containing 10% glycerol. Solubilization, protein purification via Ni²⁺-NTA, 3C protease cleavage and SEC was performed exactly as for Rv1410 purified from *E. coli* (see above).

*Hoechst 33342, ethidium and BCECF-AM transport in *L. lactis**

L. lactis NZ9000 ΔImrA ΔImrCD cells (Venter *et al.*, 2008) harboring plasmids encoding wild-type or mutant Rv1410, LmrP or MdfA were grown in GM17 Cm⁵ at 30°C. Expression was induced at an OD₆₀₀ of 0.4–0.6 with nisin (culture supernatant of *L. lactis* NZ9700) for 1 h (1:1,000 (v/v)). Cells were washed and resuspended using fluorescence

buffer (50 mM KP_i pH 7.0, 5 mM MgSO₄), adjusted to an OD₆₀₀ of 0.5 and energized by adding 0.5% glucose. Accumulation of 5 µM ethidium, 0.5 µM Hoechst 33342 at 25°C or 0.2 µM BCECF-AM at 30°C was followed for 600 s using a Fluorescence Spectrometer LS-55 (Perkin Elmer). Excitation and emission wavelengths and slit widths were set at 520, 10 and 595 nm, 15 nm for ethidium; 355, 5 and 457 nm and 5 nm for Hoechst 33342; 502, 2.5 and 525 nm, 4 nm for BCECF. Transport assays were conducted twice in two technical replicates. For clarity of discussion, one representative dataset is shown.

*Ethidium, BCECF-AM and calcein-AM transport in *M. smegmatis**

Wild-type *M. smegmatis*, *M. smegmatis* dKO (ΔMSMEG_3069-70) and *M. smegmatis* ΔlfrA (ΔMSMEG_6225) were inoculated into 25 ml of 7H9 medium and incubated at 37°C while shaking at 160 rpm until the cultures reached mid-log growth phase (OD₆₀₀ = 0.5–1.0). The cultures were harvested by centrifugation, cell pellets were resuspended in 1 ml of 50 mM potassium phosphate (KP_i) buffer (pH = 7.0) and kept on ice. Prior to the experiment, cells were diluted using KP_i buffer kept at 37°C to a final OD₆₀₀ = 0.5. 2 ml of cell suspension was transferred to a Quartz SUPRASIL® cuvette (Hellma Analytics, 101-QS) (also warmed to 37°C). The cuvette was promptly placed in a LS 55 Fluorescence Spectrometer (PerkinElmer) that was connected to a MultiTemp III water bath (Pharmacia Biotech) to keep the temperature of the cuvette at 37°C and to a magnetic stirrer (Rank Brothers Ltd, model 300) to ensure the homogeneity of the diluted culture. Before each measurement, either 0.4% w/v glucose or 500 µM carbonyl cyanide m-chlorophenyl hydrazone (CCCP) was added to the cells and incubated for 3 min while stirring. The fluorescent dyes ethidium (5 µM), BCECF-AM (0.2 µM), and calcein-AM (0.2 µM) were added 10 s after the start of fluorescence intensity measurements. Excitation and emission wavelengths and slit widths were set at 520, 10 and 595 nm, 15 nm for ethidium; at 502, 2.5 and 525 nm, 4 nm for BCECF; at 495, 12 and 520 nm, 12 nm for calcein. In the experiments shown in Fig. 4E, Glc was added, as described above, to energize the cells, but after 8 min 500 µM CCCP was added to the same sample to determine whether the presence of CCCP alters the fluorescence properties of BCECF and calcein. Average fluorescence intensities and 95% confidence intervals (using a Student's *t* distribution) were calculated from the data of six biological replicates.

*Minimal inhibitory concentration (MIC) measurements in *M. abscessus* and *M. smegmatis**

All antibiotics were purchased as powder from Sigma-Aldrich (Buchs, Switzerland) and stock solutions were prepared. Novobiocin and vancomycin were dissolved in water, rifabutin and clofazimine in DMSO, tetracycline in ethanol and ofloxacin in a 0.1 M HCl solution. The MICs for *M. abscessus* and *M. smegmatis* were performed in 96-well plates as previously described (Dal Molin *et al.*, 2018). The

MICs were determined on day 5 for *M. smegmatis* and *M. abscessus*.

Cellular growth assays in complemented M. smegmatis dKO cells

We developed a high-throughput growth assay in a 96-well format to assess the functionality of Rv1410 and LprG in *M. smegmatis* dKO cells. All tested strains (wild-type, dKO and dKO complemented with pFLAG vectors as described above) were grown to late stationary phase in 7H9 medium in the absence of antibiotics (this was possible because the pFLAG vector is stably integrated in the genome). From these pre-cultures, cells were diluted 1,000-fold into 7H9 medium containing the following drug concentrations: for the experiments assessing the operons from different mycobacteria (Figs 1D and S1): vancomycin ($0.3 \mu\text{g ml}^{-1}$), rifampicin ($0.4 \mu\text{g ml}^{-1}$), or novobiocin ($0.5 \mu\text{g ml}^{-1}$); for the experiments assessing the loop mutants (Fig. 2D–F): vancomycin ($0.0125 \mu\text{g ml}^{-1}$), rifampicin ($0.075 \mu\text{g ml}^{-1}$), or novobiocin ($0.05 \mu\text{g ml}^{-1}$). One milliliter of these cultures were transferred in 4–6 technical replicates into 96-well deep well plates and were incubated at 37°C , shaking at 300 rpm, for approximately 50 h. After removing 50 μl of each culture into 96-well plates at indicated time points, OD_{600} was measured in a microtiter plate reader (Synergy H1 Hybrid Reader, BioTek). The presented growth curves are representatives of 3 biological replicates and error bars denote the standard deviation of technical replicates.

Transmission electron microscopy

Wild-type and dKO cells were grown to stationary phase and washed in buffer. Cells were fixed with 2.5% glutaraldehyde in 0.1 M sodium cacodylate buffer (pH 7.35) for at least 1 h and sequentially treated with 1% OsO_4 for 1 h at 0°C in 0.1 M sodium cacodylate buffer and 2% uranyl acetate in H_2O for 1 h at 4°C . Pellets of bacteria were embedded in 2% of Agar, subsequently dehydrated in an ethanol series and embedded in Epon/Araldite (Sigma-Aldrich, Buchs, Switzerland). Ultrathin (50 nm) sections were contrasted with lead citrate (Reynolds) and imaged with a CM100 transmission electron microscope (Thermo Fisher Scientific, Eindhoven, The Netherlands) at an acceleration voltage of 80 KV using an Orius 1000 digital camera (Gatan, Munich, Germany).

Fluorescence microscopy

500 μl of stationary phase cultures of wild-type or dKO *M. smegmatis* carrying pLS220_Wag31-GFP (Santi *et al.*, 2013) were inoculated into 10 ml of 7H9 medium with kanamycin ($15 \mu\text{g ml}^{-1}$) (Sigma-Aldrich) and SynaptoRed C2 membrane dye ($10 \mu\text{g ml}^{-1}$) (Sigma-Aldrich) and incubated overnight at 37°C while shaking at 160 rpm until the cultures reached stationary phase ($\text{OD}_{600} = 3\text{--}5$). Experiments were conducted blinded until the last data analysis step. The stationary phase cultures were diluted 1:10 in 7H9 medium and sonicated 3 times to reduce cell

clumping (10 s $0 \times 10\%$ cycle at 80% power, Bandelin Sonopuls HD2200 sonicator). 200 μl cells were transferred on coverslips in 24 well plates and centrifuged for 10 min at 4,000 rpm and room temperature (Heraeus Multifuge 4 KR centrifuge, Thermo Scientific) to attach the mycobacterial cells to the coverslips. Cells were fixed with 4% paraformaldehyde (PFA; Electron Microscopy Sciences) for 10 min at room temperature, washed twice with 2 ml of PBS buffer, mounted on glass-slides using ProLong Diamond Antifade Mountant (Invitrogen, Thermo Fisher Scientific) and incubated at 4°C overnight. The samples were analyzed in 3D on the next day with a Leica SP8 inverse confocal laser scanning microscope (HC PL APO CS2 63x/1.4 OIL; Leica Microsystems) at excitation wavelengths of 488 and 561 nm to detect GFP and SynaptoRed respectively. The pictures were analyzed in a semi-automated workflow employing Fiji image processing package (Schindelin *et al.*, 2012) and a custom script by Dr. Moritz Kirschmann (ZMB, UZH, Switzerland). In this image analysis pipeline, consecutive poles or septa (labeled by fluorescence via Wag31-GFP fusion protein) of individual cell chains were marked manually. Each cell (chain) was saved as a region of interest (ROI) and the program calculated the number of cells per cell chain. Only cells that had been stained by SynaptoRed and harbored at least two Wag31-GFP foci on the cell poles were counted. Cells that were clustered or did not have defined boundaries on the 3D pictures were excluded from the analysis. After having counted the cells per cell chains from two biological replicates, the samples were de-blinded and data analysis was conducted using statistics software R (www.R-project.org). The cell chains, whose length was longer than 2 cells, were binned together and Pearson's χ^2 test was performed to evaluate the difference of distribution of cell chain lengths in the two strains.

Correlated optical fluorescence microscopy (OFM) and atomic force microscopy (AFM)

For AFM experiments, *M. smegmatis* wild-type and dKO strains were grown in Middlebrook 7H9 liquid medium (Difco) supplemented with 0.5% albumin, 0.2% glucose, 0.085% NaCl, 0.5% glycerol and 0.05% Tween-80. In order to conduct AFM measurements of wild-type and dKO strains in parallel under identical experimental settings, wild-type *M. smegmatis* was differentiated from dKO cells by expressing Wag31-GFP or Wag31-mCherry fusion protein from an ectopic locus, integrated at *attB*, as described previously (Santi *et al.*, 2013). Polydimethylsiloxane (PDMS)-coated coverslips were prepared by spin-coating a mixture of PDMS at a ratio of 15:1 (elastomer:curing agent) with hexane (Sigma 296090) at a ratio of 1:10 (PDMS:hexane) (Thangawng *et al.*, 2007; Koschwanez *et al.*, 2009). An aliquot of bacteria was grown to mid-exponential phase and 2–5 ml of culture was filtered (5 μm pore size PVDF filter – Millipore) to select for individual cells and concentrated to 50 μl . Wild-type cells expressing Wag31-GFP or Wag31-mCherry were mixed with the non-fluorescent dKO mutant, deposited onto the PDMS-coated coverslip and incubated for ~20 min to increase surface interactions between the hydrophobic

bacterial surface and the coverslip. Correlated optical fluorescence and AFM images were acquired as described in Eskandarian *et al.* (2017). Optical fluorescence images were acquired with an electron-multiplying charge-coupled device (EMCCD) iXon Ultra 897 camera (Andor), mounted on an IX81 inverted optical microscope (Olympus), and equipped with an UPLFLN100XO2PH \times 100 oil immersion objective (Olympus). Transmitted light illumination was provided by a 12V/100W AHS-LAMP halogen lamp. A U-MGFPHQ fluorescence filter cube for GFP with HQ-Ion-coated filters was used together with a bandpass barrier filter, exciter filter BP460-480HQ, a dichroic beam splitter DM485, and barrier filter BA495-540HQ to detect green and red fluorescence originating from Wag31-GFP and Wag31-mCherry fusion protein respectively. The AFM was mounted on top of the inverted microscope and 7H9 medium (\sim 3 ml) was supplied to the sample to immerse the bacterial sample and the AFM cantilever in fluid. Images were acquired with a Dimension Icon scan head (Bruker) using ScanAsyst fluid cantilevers (Bruker) with a nominal spring constant of 0.7 N m $^{-1}$ in Peak Force QNM mode at a force setpoint \sim 1nN and typical scan rates of 0.5 Hz. Indentation on the cell surface was estimated to be \sim 10 nm with a range of \sim 5 nm in the Z-axis. Height, peak force error, DMT modulus, and log DMT modulus were recorded for all scanned images in the trace and retrace directions. Images were processed using Gwyddion (Department of Nanometrology, Czech Metrology Institute - <http://gwyddion.net>). ImageJ was used for extracting bacterial cell profiles in a tabular form. The data were analyzed using a two-sided Wilcoxon rank sum test with continuity correction and confidence level of 95% using statistics software R (www.R-project.org).

Data availability

AFM raw data are available at: <https://figshare.com/s/088396e3e85b87530455>, DOI:10.6084/m9.figshare.7364810.

Acknowledgements

Urs Ziegler and Andres Käch of the Center for Microscopy and Image Analysis, University of Zurich, are acknowledged for collecting transmission electron microscopy images and for their help to establish the fluorescence microscopy analysis with *M. smegmatis*. Moritz Kirschmann (Center for Microscopy and Image Analysis, University of Zurich) is acknowledged for his help during data analysis of fluorescence microscopy images. We thank Märt Möls (University of Tartu) for his advice on statistical analysis of fluorescence microscopy data. We thank Stefan Schauer of the Functional Genomics Center Zurich for his support during SPR measurements. All members of the Seeger lab are acknowledged for project discussion. Work in the lab of MAS was supported by a SNSF Professorship of the Swiss National Science Foundation (PP00P3_144823), the European Research Council (ERC) (consolidator grant n° 772190) and a grant of the Novartis Foundation for Medical-Biological

Research (to MAS). SR and FMA were supported by two Cando fellowships of the University of Zurich. P.S. was supported by the Swiss National Science Foundation (SNSF; #31003A_153349/1), the Baugarten Stiftung (STWF-18-011), and the Swiss Lung Association (SLA: 2018-02). HAE was supported by a European Molecular Biology Organization advanced Long Term Fellowship (EMBO ALTF 191-2014 and aALTF 750-2016). AFM work was funded by grants to GEF from the European Union FP7/2007–2013/ERC under grant agreement no. 307338-NaMic, and the European Research Council (ERC) (consolidator grant No: 773091).

Author contributions

MH, SR, PS and MAS conceived the project. MAS generated the homology model. MH generated *M. smegmatis* dKO and cloned all genes into the respective complementation and expression vectors for *E. coli* and mycobacteria and MH and SR carried out mutagenesis. MH purified Rv1410, Rv1410 loop truncations and LprG and conducted SPR experiments. SR determined MIC and performed growth experiments in *M. smegmatis*. MDM generated *M. abscessus* dKO and performed MIC determinations in *M. abscessus*. SR carried out dye transport experiments in *M. smegmatis* and *L. lactis*. HAE performed AFM experiments. SR performed and analyzed fluorescence microscopy experiments. MH prepared the samples for TEM. FMA generated *M. smegmatis* *ΔlfrA*. LMH and AK cloned transporters into *L. lactis*, performed transport experiments in *L. lactis*, determined expression levels of GFP-fusion proteins and purified Rv1410 from *L. lactis*. MH, SR, HAE, MDM, LMH, AK, PS and MAS analyzed and interpreted the data. MH, LMH, GEF, PS and MAS supervised students and postdocs. MH, SR, HAE and MAS wrote the paper. MDM and PS edited the paper.

References

- Arnold, F.M., Hohl, M., Remm, S., Koliwer-Brandl, H., Adenau, S., Chusri, S., *et al.* (2018) A uniform cloning platform for mycobacterial genetics and protein production. *Scientific Reports*, **8**(1):9539.
- Biasini, M., Bienert, S., Waterhouse, A., Arnold, K., Studer, G., Schmidt, T., *et al.* (2014) SWISS-MODEL: modelling protein tertiary and quaternary structure using evolutionary information. *Nucleic Acids Research*, **42**, W252–W258.
- Bigi, F., Alito, A., Romano, M.I., Zumarraga, M., Caimi, K. and Cataldi, A. (2000) The gene encoding P27 lipoprotein and a putative antibiotic-resistance gene form an operon in *Mycobacterium tuberculosis* and *Mycobacterium bovis*. *Microbiology*, **146**(Pt 4), 1011–1018.
- Bigi, F., Gioffre, A., Klepp, L., Santangelo, M.P., Alito, A., Caimi, K., *et al.* (2004) The knockout of the *lprG-Rv1410*

- operon produces strong attenuation of *Mycobacterium tuberculosis*. *Microbes and Infection*, **6**, 182–187.
- Boens, N., Qin, W., Basaric, N., Orte, A., Talavera, E.M. and Alvarez-Pez, J.M. (2006) Photophysics of the fluorescent pH indicator BCECF. *The Journal of Physical Chemistry A*, **110**, 9334–9343.
- Brosch, R., Gordon, S.V., Billault, A., Garnier, T., Eglmeier, K., Soravito, C., et al. (1998) Use of a *Mycobacterium tuberculosis* H37Rv bacterial artificial chromosome library for genome mapping, sequencing, and comparative genomics. *Infection and Immunity*, **66**, 2221–2229.
- Brown-Elliott, B.A., Nash, K.A. and Wallace, R.J. (2012) Antimicrobial susceptibility testing, drug resistance mechanisms, and therapy of infections with nontuberculous mycobacteria. *Clinical Microbiology Reviews*, **25**, 545–582.
- Bukowska, M.A., Hohl, M., Geertsma, E.R., Hürlimann, L.M., Grütter, M.G. and Seeger, M.A. (2015) A transporter motor taken apart: flexibility in the nucleotide binding domains of a heterodimeric ABC exporter. *Biochemistry*, **54**, 3086–3099.
- Cull, M.G. and Schatz, P.J. (2000) Biotinylation of proteins *in vivo* and *in vitro* using small peptide tags. *Methods in Enzymology*, **326**, 430–440.
- Dal Molin, M., Gut, M., Rominski, A., Haldimann, K., Becker, K. and Sander, P. (2018) Molecular mechanisms of intrinsic streptomycin resistance in *Mycobacterium abscessus*. *Antimicrobial Agents and Chemotherapy*, **62**:e01427-17.
- Dhiman, R.K., Dinadayala, P., Ryan, G.J., Lenaerts, A.J., Schenkel, A.R. and Crick, D.C. (2011) Lipooligosaccharide localization and abundance during growth of *Mycobacterium smegmatis*. *Journal of Bacteriology*, **193**, 5802–5809.
- Drage, M.G., Tsai, H.C., Pecora, N.D., Cheng, T.Y., Arida, A.R., Shukla, S., et al. (2010) *Mycobacterium tuberculosis* lipoprotein LprG (Rv1411c) binds triacylated glycolipid agonists of Toll-like receptor 2. *Nature Structural & Molecular Biology*, **17**, 1088–1095.
- Eskandarian, H.A., Odermatt, P.D., Ven, J.X.Y., Hannebelle, M.T.M., Nievergelt, A.P., Dhar, N., et al. (2017) Division site selection linked to inherited cell surface wave troughs in mycobacteria. *Nature Microbiology*, **2**, 17094.
- Farrow, M.F. and Rubin, E.J. (2008) Function of a mycobacterial major facilitator superfamily pump requires a membrane-associated lipoprotein. *Journal of Bacteriology*, **190**, 1783–1791.
- Gaur, R.L., Ren, K.N., Blumenthal, A., Bhamidi, S., Gibbs, S., Jackson, M., et al. (2014) LprG-mediated surface expression of lipooligosaccharide is essential for virulence of *Mycobacterium tuberculosis*. *PLoS Pathogens*, **10** (9):e1004376.
- Geertsma, E.R. and Dutzler, R. (2011) A versatile and efficient high-throughput cloning tool for structural biology. *Biochemistry*, **50**, 3272–3278.
- Geertsma, E.R. and Poolman, B. (2007) High-throughput cloning and expression in recalcitrant bacteria. *Nature Methods*, **4**, 705–707.
- Guettou, F., Quistgaard, E.M., Trasauques, L., Moberg, P., Jegerschold, C., Zhu, L., et al. (2013) Structural insights into substrate recognition in proton-dependent oligopeptide transporters. *EMBO Reports*, **14**, 804–810.
- Hoffmann, C., Leis, A., Niederweis, M., Plitzko, J.M. and Engelhardt, H. (2008) Disclosure of the mycobacterial outer membrane: cryo-electron tomography and vitreous sections reveal the lipid bilayer structure. *Proceedings of the National Academy of Sciences of the United States of America*, **105**, 3963–3967.
- Hürlimann, L.M., Corradi, V., Hohl, M., Bloomberg, G.V., Tielemans, D.P. and Seeger, M.A. (2016) The heterodimeric ABC transporter EfrCD mediates multidrug efflux in *Enterococcus faecalis*. *Antimicrobial Agents and Chemotherapy*, **60**, 5400–5411.
- Koschwanez, J.H., Carlson, R.H. and Meldrum, D.R. (2009) Thin PDMS films using long spin times or tert-butyl alcohol as a solvent. *PLoS ONE*, **4**(2):e4572.
- Luthra, S., Rominski, A. and Sander, P. (2018) The role of antibiotic-target-modifying and antibiotic-modifying enzymes in *Mycobacterium abscessus* drug resistance. *Frontiers in Microbiology*, **9**, 2179.
- Martinot, A.J., Farrow, M., Bai, L., Layre, E., Cheng, T.Y., Tsai, J.H., et al. (2016) Mycobacterial metabolic syndrome: LprG and Rv1410 regulate triacylglyceride levels, growth rate and virulence in *Mycobacterium tuberculosis*. *PLoS Pathogens*, **12**(1):e1005351.
- Masureel, M., Martens, C., Stein, R.A., Mishra, S., Ruysschaert, J.M., McHaourab, H.S., et al. (2014) Protonation drives the conformational switch in the multidrug transporter LmrP. *Nature Chemical Biology*, **10**, 149–155.
- Mazurkiewicz, P., Poelarends, G.J., Driessens, A.J. and Konings, W.N. (2004) Facilitated drug influx by an energy-uncoupled secondary multidrug transporter. *Journal of Biological Chemistry*, **279**, 103–108.
- Mougari, F., Guglielmetti, L., Raskine, L., Sermet-Gaudelus, I., Veziris, N. and Cambau, E. (2016) Infections caused by *Mycobacterium abscessus*: epidemiology, diagnostic tools and treatment. *Expert Review of Anti-infective Therapy*, **14**, 1139–1154.
- Newstead, S. (2015) Molecular insights into proton coupled peptide transport in the PTR family of oligopeptide transporters. *Biochimica et Biophysica Acta (BBA) – General Subjects*, **1850**, 488–499.
- Nikaido, H. (2005) Restoring permeability barrier function to outer membrane. *Chemistry & Biology*, **12**, 507–509.
- Normark, S., Boman, H.G. and Matsson, E. (1969) Mutant of *Escherichia coli* with anomalous cell division and ability to decrease episomally and chromosomally mediated resistance to ampicillin and several other antibiotics. *Journal of Bacteriology*, **97**, 1334–1342.
- Okuda, S., Sherman, D.J., Silhavy, T.J., Ruiz, N. and Kahne, D. (2016) Lipopolysaccharide transport and assembly at the outer membrane: the PEZ model. *Nature Reviews Microbiology*, **14**, 337–345.
- Ozkan, P. and Mutharasan, R. (2002) A rapid method for measuring intracellular pH using BCECF-AM. *Biochimica et Biophysica Acta (BBA) - General Subjects*, **1572**, 143–148.
- Paulsen, I.T., Brown, M.H., Littlejohn, T.G., Mitchell, B.A. and Skurray, R.A. (1996a) Multidrug resistance proteins QacA and QacB from *Staphylococcus aureus*: membrane

- topology and identification of residues involved in substrate specificity. *Proceedings of the National Academy of Sciences of the United States of America*, **93**, 3630–3635.
- Paulsen, I.T., Brown, M.H. and Skurray, R.A. (1996b) Proton-dependent multidrug efflux systems. *Microbiological Reviews*, **60**, 575–608.
- Perkins, H.R. (1969) Specificity of combination between mucopeptide precursors and vancomycin or ristocetin. *Biochemical Journal*, **111**, 195–205.
- Ramon-Garcia, S., Martin, C., Thompson, C.J. and Ainsa, J.A. (2009) Role of the *Mycobacterium tuberculosis* P55 efflux pump in intrinsic drug resistance, oxidative stress responses, and growth. *Antimicrobial Agents and Chemotherapy*, **53**, 3675–3682.
- Reddy, V.S., Shlykov, M.A., Castillo, R., Sun, E.I. and Saier, M.H., Jr. (2012) The major facilitator superfamily (MFS) revisited. *FEBS Journal*, **279**, 2022–2035.
- Rodrigues, L., Ramos, J., Couto, I., Amaral, L. and Viveiros, M. (2011) Ethidium bromide transport across *Mycobacterium smegmatis* cell-wall: correlation with antibiotic resistance. *BMC Microbiology*, **11**, 35.
- Rominski, A., Roditscheff, A., Selchow, P., Bottger, E.C. and Sander, P. (2017) Intrinsic rifamycin resistance of *Mycobacterium abscessus* is mediated by ADP-ribosyltransferase MAB_0591. *Journal of Antimicrobial Chemotherapy*, **72**, 376–384.
- Sander, P., De Rossi, E., Boddinghaus, B., Cantoni, R., Branzoni, M., Bottger, E.C., et al. (2000) Contribution of the multidrug efflux pump LfrA to innate mycobacterial drug resistance. *FEMS Microbiology Letters*, **193**, 19–23.
- Santi, I., Dhar, N., Bousbaine, D., Wakamoto, Y. and McKinney, J.D. (2013) Single-cell dynamics of the chromosome replication and cell division cycles in mycobacteria. *Nature Communications*, **4**, 2470.
- Schindelin, J., Arganda-Carreras, I., Frise, E., Kaynig, V., Longair, M., Pietzsch, T., et al. (2012) Fiji: an open-source platform for biological-image analysis. *Nature Methods*, **9**, 676–682.
- Seeger, M.A., Mittal, A., Velamakanni, S., Hohl, M., Schauer, S., Salaa, I., et al. (2012) Tuning the drug efflux activity of an ABC transporter *in vivo* by *in vitro* selected DARPin binders. *PLoS ONE*, **7**, e37845.
- Shukla, S., Richardson, E.T., Athman, J.J., Shi, L., Wearsch, P.A., McDonald, D., et al. (2014) *Mycobacterium tuberculosis* lipoprotein LprG binds lipoarabinomannan and determines its cell envelope localization to control phagolysosomal fusion. *PLoS Pathogens*, **10**, e1004471.
- Shukla, S., Richardson, E.T., Drage, M.G., Boom, W.H., and Harding, C.V. (2018). *Mycobacterium tuberculosis* lipoprotein and lipoglycan binding to toll-like receptor 2 correlates with agonist activity and functional outcomes. *Infection and Immunity*, **86**(10), pii: e00450-18.
- Sigal, N., Molshanski-Mor, S. and Bibi, E. (2006) No single irreplaceable acidic residues in the *Escherichia coli* secondary multidrug transporter MdfA. *Journal of Bacteriology*, **188**, 5635–5639.
- Silva, P.E.A., Bigi, F., Santangelo, M.D., Romano, M.I., Martin, C., Cataldi, A., et al. (2001) Characterization of P55, a multidrug efflux pump in *Mycobacterium bovis* and *Mycobacterium tuberculosis*. *Antimicrobial Agents and Chemotherapy*, **45**, 800–804.
- Springer, B., Sander, P., Sedlacek, L., Ellrott, K. and Bottger, E.C. (2001) Instability and site-specific excision of integration-proficient mycobacteriophage L5 plasmids: development of stably maintained integrative vectors. *International Journal of Medical Microbiology*, **290**, 669–675.
- Stanley, N.R., Findlay, K., Berks, B.C. and Palmer, T. (2001) *Escherichia coli* strains blocked in Tat-dependent protein export exhibit pleiotropic defects in the cell envelope. *Journal of Bacteriology*, **183**, 139–144.
- Takechi-Haraya, Y., Sakai-Kato, K. and Goda, Y. (2017) Membrane rigidity determined by atomic force microscopy is a parameter of the permeability of liposomal membranes to the hydrophilic compound calcein. *AAPS PharmSciTech: An Official Journal of the American Association of Pharmaceutical Scientists*, **18**, 1887–1893.
- Thangawng, A.L., Ruoff, R.S., Swartz, M.A. and Glucksberg, M.R. (2007) An ultra-thin PDMS membrane as a bio/micro-nano interface: fabrication and characterization. *Biomedical Microdevices*, **9**, 587–595.
- Touchette, M.H., Van Vlack, E.R., Bai, L., Kim, J., Cognetta, A.B., Previti, M.L., et al. (2017) A screen for protein–protein interactions in live mycobacteria reveals a functional link between the virulence-associated lipid transporter LprG and the mycolyltransferase antigen 85A. *ACS Infectious Diseases*, **3**, 336–348.
- Venter, H., Velamakanni, S., Balakrishnan, L. and van Veen, H.W. (2008) On the energy-dependence of Hoechst 33342 transport by the ABC transporter LmrA. *Biochemical Pharmacology*, **75**, 866–874.
- Vorachek-Warren, M.K., Carty, S.M., Lin, S., Cotter, R.J. and Raetz, C.R. (2002) An *Escherichia coli* mutant lacking the cold shock-induced palmitoleyltransferase of lipid A biosynthesis: absence of unsaturated acyl chains and antibiotic hypersensitivity at 12 degrees C. *Journal of Biological Chemistry*, **277**, 14186–14193.
- Weigand, R.A., Vinci, K.D. and Rothfield, L.I. (1976) Morphogenesis of bacterial division septum – new class of septation-defective mutants. *Proceedings of the National Academy of Sciences of the United States of America*, **73**, 1882–1886.
- Yakushi, T., Masuda, K., Narita, S., Matsuyama, S. and Tokuda, H. (2000) A new ABC transporter mediating the detachment of lipid-modified proteins from membranes. *Nature Cell Biology*, **2**, 212–218.
- Young, K. and Silver, L.L. (1991) Leakage of periplasmic enzymes from envA strains of *Escherichia coli*. *Journal of Bacteriology*, **173**, 3609–3614.
- Young, K., Silver, L.L., Bramhill, D., Cameron, P., Eveland, S.S., Raetz, C.R.H., et al. (1995) The envA permeability cell division gene of *Escherichia coli* encodes the second enzyme of lipid A biosynthesis - UDP-3-O-(R-3-hydroxymyristoyl)-N-acetylglucosamine deacetylase. *Journal of Biological Chemistry*, **270**, 30384–30391.

Supporting information

Additional supporting information may be found online in the Supporting Information section at the end of the article.